

Article

TSR action and genesis mechanism of antimony deposit: Evidence from aromatic hydrocarbon geochemistry of bitumen in paleo-oil reservoir near Qinglong ore field, Southwestern Guizhou Depression, China

Yong Cheng^{1,2}, Yuzhao Hu^{1,*}, Saihua Xu¹, Di Wang³

¹ Faculty of Land and Resource Engineering, Kunming University of Science and Technology, Kunming 650093, Yunnan, China; cheng_yong1988@163.com (Y. C.); xusaihua18@126.com (S. X.)

² Faculty of Metallurgy and Mining Engineering, Kunming Metallurgy College, Kunming 650033, Yunnan, China

³ School of Earth Sciences and Resources, China University of Geosciences, Beijing 100083, PR China; shadywangdi@gmail.com

* Correspondence: huyuzhao155@sohu.com

Abstract: In Qinglong ore field, paleo-oil reservoir is found to be associated with antimony deposits, and they have close genetic relationship. In this study, aromatics geochemistry of paleo-oil reservoir bitumen was studied to further discuss the thermochemical sulfate reduction (TSR) reaction and the mechanism of antimony mineralization. A total of 124 aromatic compounds were identified by Gas chromatography-mass spectrometry (GC-MS) analysis in bitumen samples, including abundant phenanthrene series, dibenzothiophene series, fluoranthene series, chrysene series, and a small number of fluorene series, naphthalene series, dibenzofuran series, biphenyl series, triaromatic steroid series. Aromatic parameters such as trimethylnaphthalene index (TMNr), methylphenanthrene index (MPI), methylphenanthrene distribution fraction (MPDF, F₁ and F₂), methyl dibenzothiophene parameter (MDR), C₂₈TAS-20S/(20R+20S), and benzo[fluoranthene]/benzo[e]pyrene indicate Qinglong paleo-oil reservoir is in over maturity level. The abundance of phenanthrene and chrysene aromatic compounds and a small amount of naphthalene series, benzo[fluoranthene], fluoranthene, pyrene, anthracene, retene, perylene and biphenyl suggest that the parent material of the paleo-oil reservoir was mainly low aquatic organisms, mixed with a small amount of higher plant. The detected a certain number of compounds, such as retene, triaromatic steroid series and perylene, the ternary diagram of DBF-DBT-F and binary plot of Pr/Ph-DBT/P, DBT/(F+DBT)-DBF/(F+DBF) and Pr/Ph-DBT/DBF reveal that the source rock of the paleo-oil reservoir was formed in the marine environment of weak oxidation and weak reduction. The comprehensive analysis shows that the Qinglong paleo-oil reservoir originated from Devonian source rocks, just like other paleo-oil reservoirs and natural gas reservoirs in the Nanpanjiang basin. Abundant dibenzothiophene series were detected, indicating that the paleo-oil reservoir underwent a certain degree of TSR reaction. We believe that the paleo-gas reservoir formed by the evolution of paleo-oil reservoir participated in antimony mineralization, that is, hydrocarbon organic matter acted as reducing agent and transformed SO₄²⁻ in oilfield brine into H₂S through TSR, providing reduced sulfur and creating environmental conditions for mineralization.

Keywords: palaeo-oil reservoir; aromatic hydrocarbons; thermochemical sulphate reduction (TSR); Qinglong antimony deposit; Nanpanjiang basin

1. Introduction

Sedimentary basin is a huge complex system in which a variety of organic and inorganic, metallic and nonmetallic mineral resources and water resources coexist [1]. As the phenomenon of close paragenesis or associated occurrence between metal deposits and

hydrocarbon organic matter has been discovered [2–12], the relationship between metal mineralization and hydrocarbon accumulation has attracted more and more attention of mineral deposit scholars, and the study of organic-inorganic interaction and mineralization effect in sedimentary basins has been aroused [13–18].

Qinglong antimony ore field is located on southwest Guizhou depression of Nanpanjiang basin, and its antimony metal reserves (~ 0.21Mt) rank fifth in south China giant antimony metallogenic belt [19–21] (Figure 1). The characteristics of the deposit, ore-forming materials, ore-forming fluids, and ore-forming age have been studied deeply by predecessors [22–33]. As early as in the 1990s, some scholars reported that the Qinglong antimony deposit is rich in organic inclusions, and speculated that its formation is related to organic matter [34–35]. Since no large-scale organic geological bodies had been found, the further study on the genetic relationship between organic matter and antimony deposit was limited. Fortunately, in 2012, our team found a paleo-oil reservoir in the Shailing ore block when we were prospecting outside the Qinglong antimony deposit [36–37], which created conditions for further discussion on the relationship between organic matter and antimony mineralization.

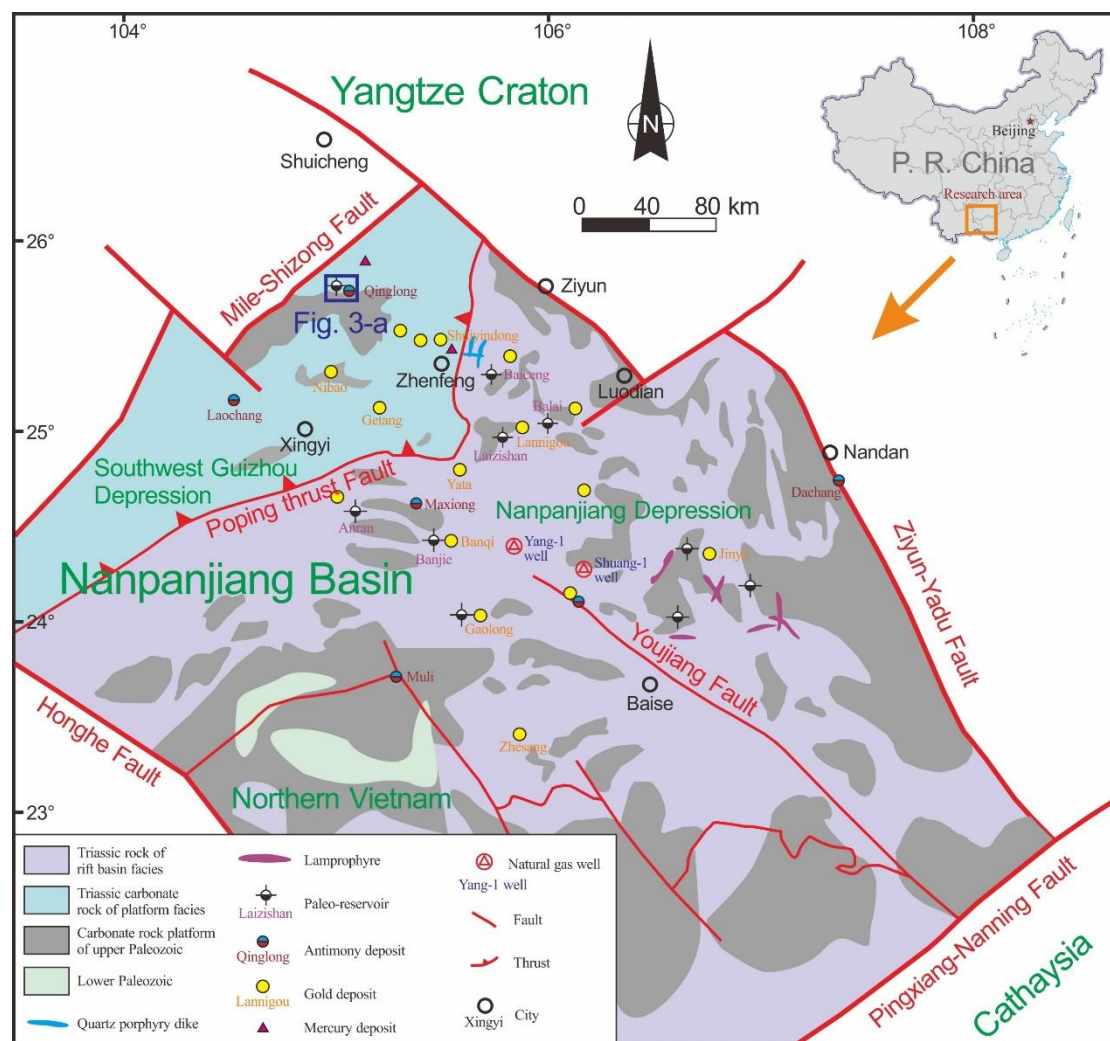


Figure 1. Simplified geologic map, showing the distribution of tectonic units and Au-Sb deposits in the Nanpanjiang basin, SW China (modified after [40]).

Our team has carried out some research work on paleo-oil reservoir bitumen, including physical characteristics and genesis of bitumen, element geochemistry, organic geochemistry, S-C isotope, inclusion, Re-Os isotope dating and its relationship with antimony deposit [36–40]. Based on the data, we believe that hydrocarbon organic matter is involved in antimony mineralization and contributes a large amount of reduced sulfur to antimony mineralization through thermochemical sulfate reduction (TSR) reaction [38–40].

However, some scholars hold a different view and believe that S originated from magma [22,27]. In this study, aromatics geochemistry of paleo-oil reservoir bitumen was studied to further discuss the TSR reaction and the mechanism of antimony mineralization.

2. Geological background

2.1 Regional geology

The Nanpanjiang Basin (also referred to as the the Youjiang Basin or Nanpanjiang-Youjiang Basin in some references) belongs to the South China fold system, which is located at the southwestern margin of the Yangtze Block and extends from Southwest China to North Vietnam (Figure 1). The Nanpanjiang Basin hosts many Au-Sb-As-Hg deposits, which is an important part of the low-temperature metallogenic domain in southwest China [41]. The basin is significantly influenced by deep-seated faults, and its margins are controlled by three faults and a shear zone, which are NE-striking Mile-Shizong fault, NW-striking Ziyun-Yadu fault, NE-striking Pingxiang-Nanning fault, and SW Honghe shear zone [42]. There are NW-striking, NE-striking, NEE-striking and EW-striking faults in the basin, among which NW-striking faults are dominant.

Geophysical data reveal that the Nanpanjiang Basin may have three sets of basements, namely Paleoproterozoic crystalline basement, Mesoproterozoic shallow metamorphic basement and early Paleozoic fold basement [43]. The cover of the basin is Devonian to Triassic. Bounded by Poping thrust fault, Nanpanjiang Basin can be divided into Southwest Guizhou depression in the northwest and Nanpanjiang Depression in the southeast [44] (Figure 1). The southwest Guizhou Depression is a platform facies area with shallow platform carbonate rocks and impurity carbonate rocks intercalated with clastic rocks from Upper Paleozoic to Mesozoic. The Nanpanjiang depression is a basin facies area, which is characterized by the flysch formation clastic rocks of the Triassic. Isolated platform carbonate rocks of Carboniferous and Permian are also distributed sporadically in the basin.

The magmatic activity in Nanpanjiang basin is not particularly developed and there are multi-stage igneous rocks from Hercynian period to Yanshan Period [27]. The volcanic activity in the basin is weak, and there are only a few basic-ultrabasic rocks. The volcanic activity in the basin margin is more frequent, and there are a lot of basic rocks and a small number of intermediate-acid rocks and ultra-basic rocks.

Au-Sb deposits occur mainly in the Permian to Middle Triassic impure carbonate rocks and terrigenous fine clastic rocks, and often coexist with or adjacent to paleo-oil reservoirs, remnant oil and gas, and bitumen in the Permian reef and shoal carbonate rocks in space (Figure 1). The host rocks and ores of these deposits are characterized by rich organic matter, and the hydrothermal minerals of the ore often contain rich bitumen and hydrocarbon organic inclusions, indicating a close genetic relationship between gold and antimony mineralization and oil and gas accumulation [9,38].

2.2 Deposit geology

The Qinglong antimony ore field is located in southwest Guizhou Depression (Figure 1). Its tectonic evolution had experienced the formation of basement and palaeohigh in pre-Devonian, extension structure in Devonian to Middle Triassic, foreland thrust-fold structure in late Indosinian and uplift and denudation stage in Yanshanian and Himalayan period [45]. The Devonian system is dominated by limestone and dark mudstone, and the lower part of the organic-rich mudstone is a good source rock. The Carboniferous is mainly composed of dolomite, followed by limestone, with localized source rocks in the lower part. The Permian consists of limestone, volcanic rock, coal-bearing strata, and mudstone from bottom to top, with several sets of localized source rocks. The Triassic is carbonate rock and clastic rock (Figure 2).

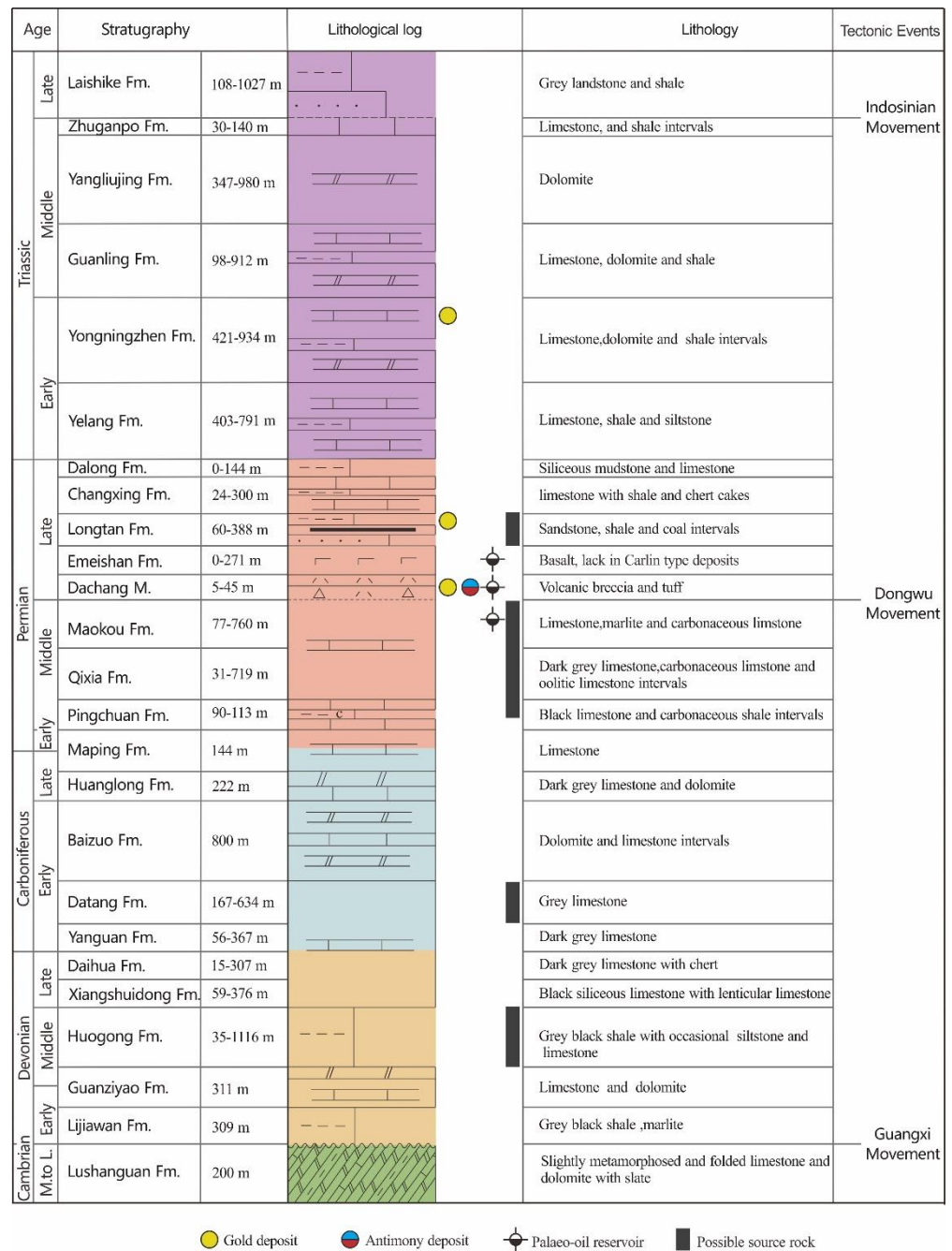


Figure 2. The stratigraphic sequences of central Southwestern Guizhou (modified after [45]).

The strata exposed in Qinglong antimony ore field are mainly Permian, including middle Permian Maokou Formation limestone (P_{2m}), "Danchang layer" (P_{3d}), Upper Permian Emeishan basalts ($P_{3\beta}$) and Upper Permian Longtan Formation coal-bearing strata (P_{3l}) from old to new [38] (Figure 3). The ore field is obviously controlled by NE-striking structure. The spatial distribution of basalt and antimony deposits in this area is controlled by the High-angle thrust fault of Huayujing fault and Qingshanzhen fault [40].

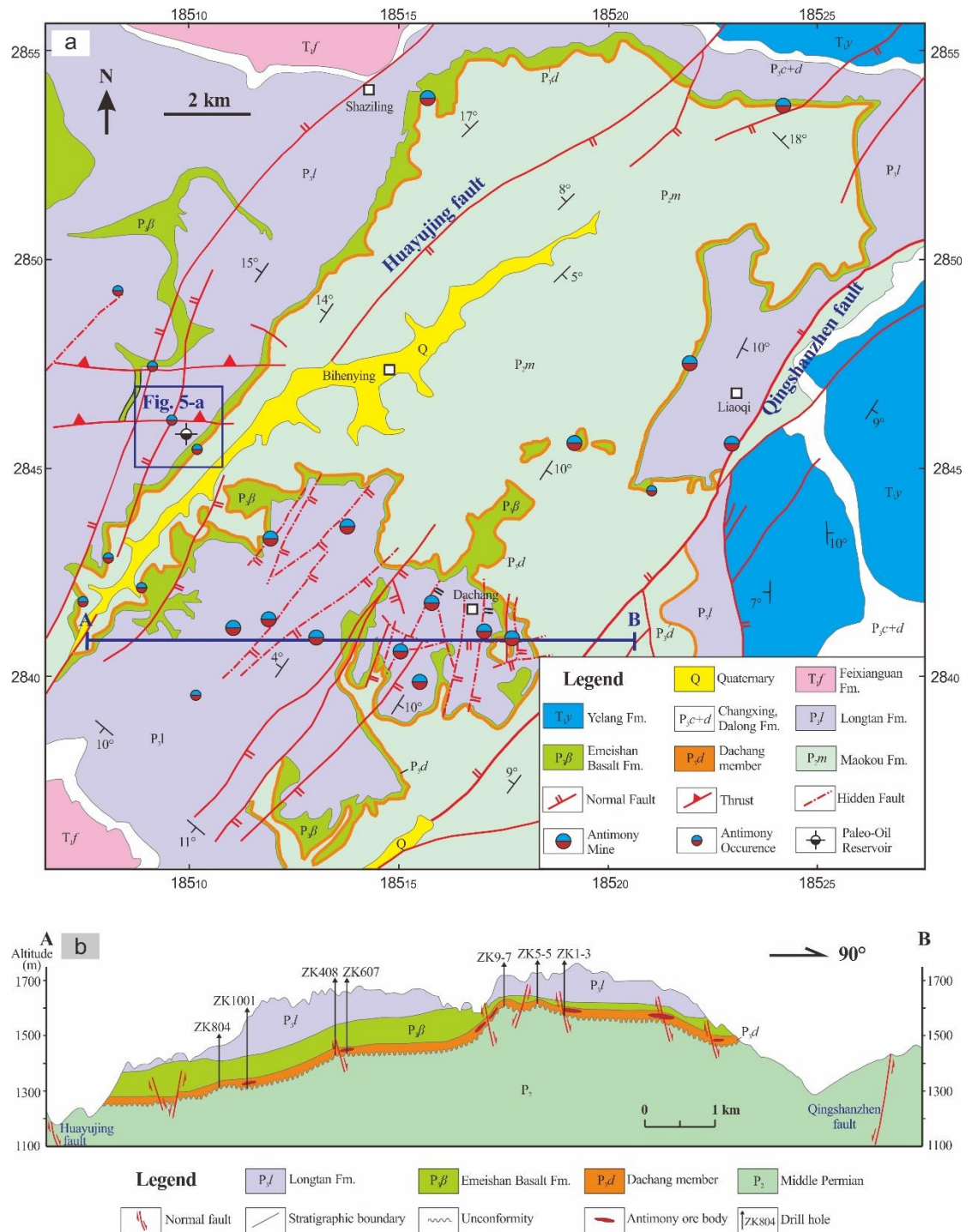


Figure 3. Geological map of Qinglong antimony ore field (a) and geological section map (b) (modified after [40]).

The antimony ore body mainly occurs in the "Dachang layer", a set of siliceous altered rocks between the Maokou Formation and the Emeishan basalts (Figure 4). "Dachang layer" is not a formal rock stratigraphic unit in the region, but an important marker bed in the mining area. According to lithology, it can be divided into three units: the lower unit is the strong silicified rock, and the top of the brecciated strong silicified rock is the ore-hosting part of antimony deposit; The middle unit is composed of basaltic conglomerate in which the brecciated clay stone with strong silicification is the main ore-hosting site; The upper unit is clay rock, among which alteration basalt is the ore-hosting site [27].

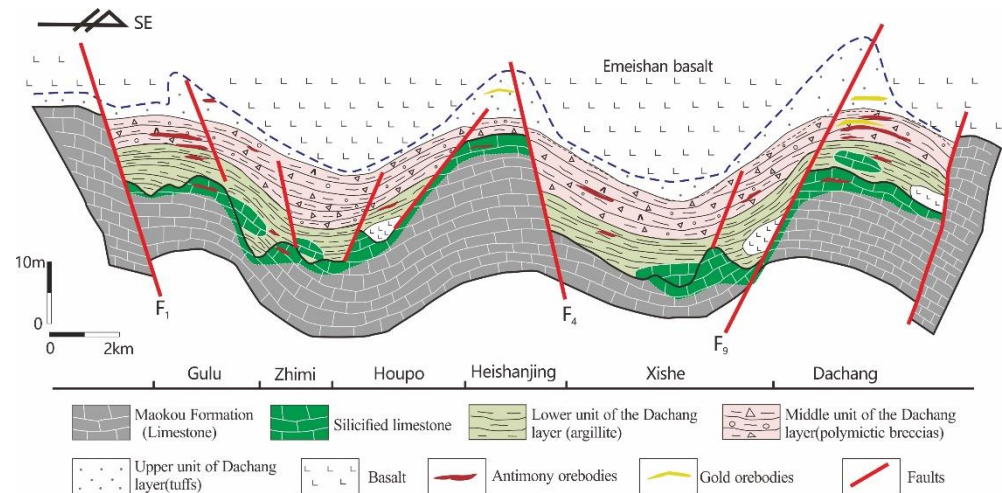


Figure 4. Lithologic variation and orebody occurrence in "Dachang layer" (modified after [27]).

The mineral assemblage of the deposit is relatively simple. The main metallic minerals are stibnite and pyrite, with a small amount of valentinite and chalcopyrite. Gangue minerals mainly include quartz, fluorite, calcite, kaolinite and a small amount of barite and gypsum. The wall rock alteration includes pyritization, silicification, fluoritization, clayzation and a little bituminization, calcilization, baratization and gypsumification.

3. Features of Qinglong paleo-oil reservoir

The paleo-oil reservoir is very close to the antimony deposit in spatial location (Figure 3). A total of fifteen layers of bitumen were found in the five exploration drill holes (ZK3506, ZK2907, ZK2303, ZK2905, ZK3101) (Figure 5). The bitumen layers mainly occur in the Upper Permian Emeishan basalt ($P_3\beta$) and a small amount in the Upper Permian "Dachang layer" volcanic breccia (P_3d) and Middle Permian Maokou formation limestone (P_2m). The thickness of bitumen layers is between 0.20 and 8.39 m, with an average of 3.3 m. The bitumen content (effective surface porosity) in the drill core is 0.5%~15.0%, with a weighted average of 4.86%. According to the estimation of experts from Sinopec, the bitumen reserve is 84×10^4 t, and its original oil reserve is about 2000×10^4 t, which is equivalent to the size of medium-scale oil field in China.

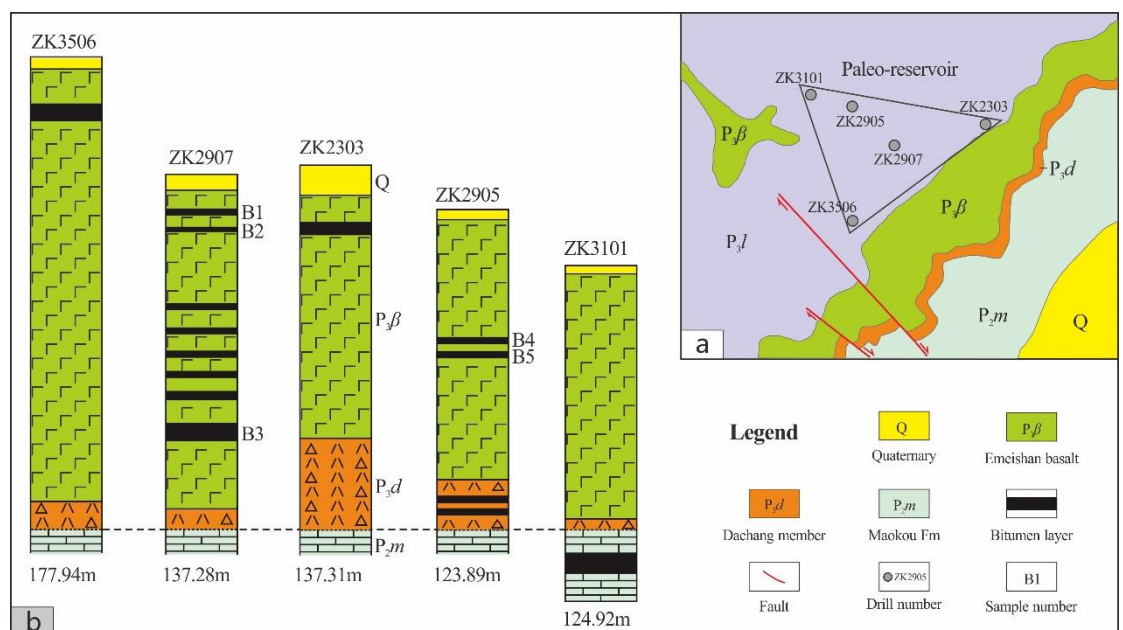


Figure 5. Sketch map of the location of the five boreholes (a) and drill columns (b) in Qinglong antimony ore field (modified after [40]).

The bitumen is black and brown, hard, brittle, hands-free, with resin luster and conchoidal fracture, and non-combustible (Figure 6a). The bitumen is mainly filled in tuff fractures or pores (Figure 6b), between volcanic breccia (Figure 6c), in the fractures or vesicles of basalt (Figure 6d), in limestone fractures or caves (Figure 6e). The paragenesis of pyrite and bitumen can be seen in hand specimens (Figure 6f). Microscopical observation also shows that bitumen is paragenetic with chalcopyrite, bornite and calcite.

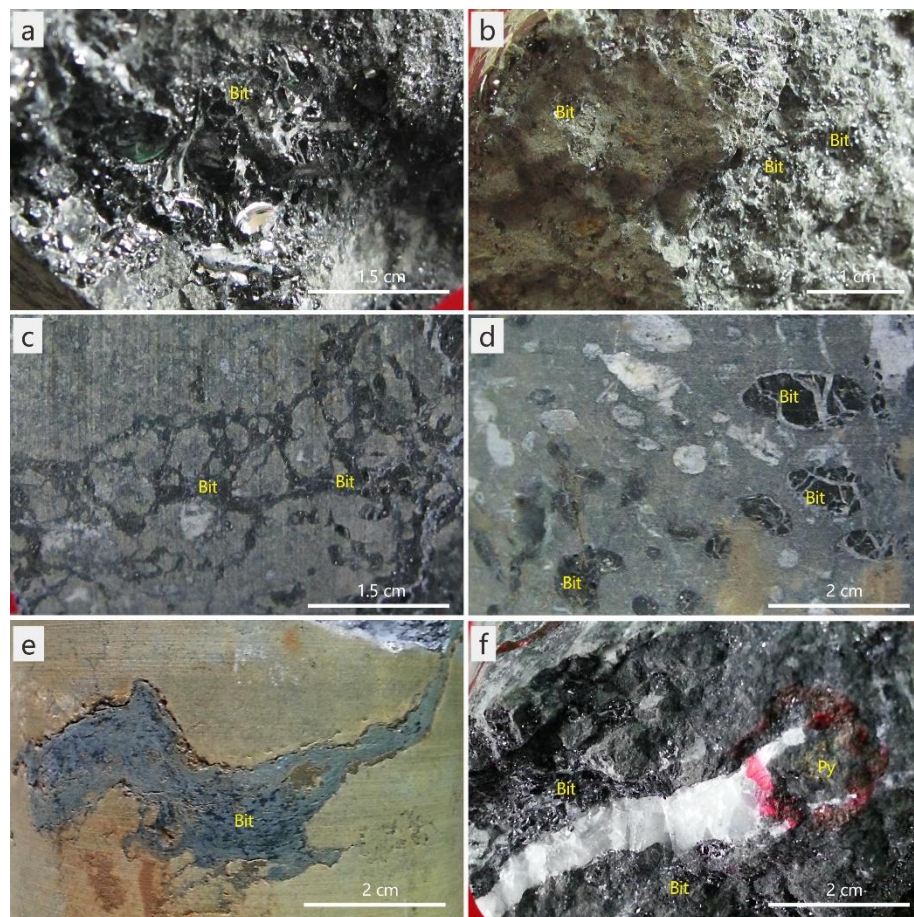


Figure 6. The distribution of bitumen in the paleo-reservoir from Qinglong antimony ore field.

(a) Black bitumen hard and brittle, with resinous luster and conchoidal fracture. (b) Bitumen in the pores of tuff. (c) Bitumen between volcanic breccia. (d) Bitumen in the vesicles of basalt. (e) Bitumen in the caverns of limestone. (f) The paragenesis of pyrite and bitumen.

Abbreviations: Bit = Bitumen; Py = Pyrite

Field work shows that solid bitumen also exists in the surrounding rock of the deposit. Solid bitumen can be seen in both the unaltered basalt and altered basalt of the “Dachang layer”. The bitumen is black granular or thin film and paragenetic with quartz, kaolinite, fluorite, and pyrite, but no paragenetic with stibnite. Therefore, it is believed that the bituminization occurred before the antimony mineralization.

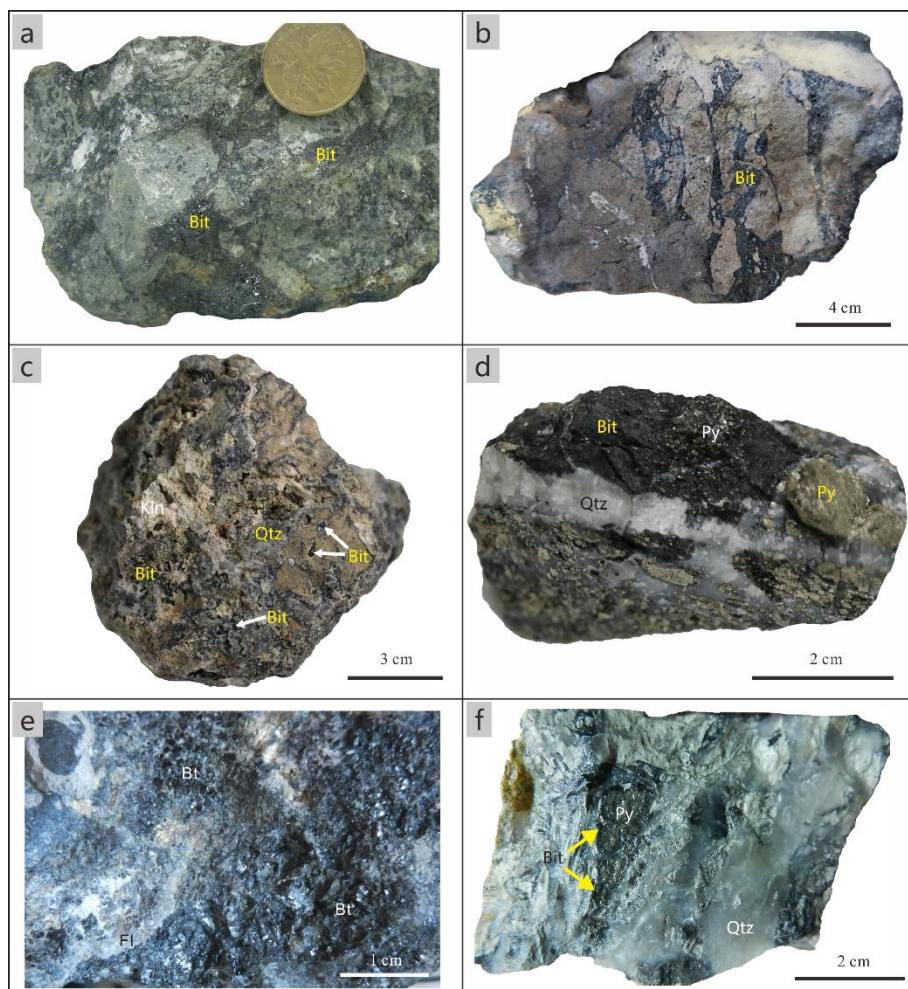


Figure 7. Characteristics of solid bitumen in surrounding rock from Qinglong antimony ore field.

a. Granular bitumen occurs in the pores of unaltered basalt in “Dachang layer”; b~f. Bitumen in altered basalt of “Dachang layer”; b. thin film bitumen distributed along basalt fissures; c. Granular bitumen is paragenetic with quartz and kaolinite; d. Lump bitumen is paragenetic with quartz and pyrite; e. Granular bitumen is paragenetic with fluorite (Quoted from [23]); f. Granular or veined bitumen is paragenetic with quartz and pyrite (Quoted from [27]). Abbreviations: Bit = Bitumen; Py = Pyrite; Kln = kaolinite; Fl = fluorite.

3 Samples and experimental methods

Five samples of bitumen were obtained from drilling cores of the paleo-oil reservoir in the Emeishan basalt. The chloroform bitumen A and its family components analysis shows that the aromatic fraction of bitumen samples accounts for 20.51~25.00% of soluble components, with an average of 23.09% [40] (Figure 8).

The aromatic compounds were analysed by gas chromatography-mass spectrometry (GC-MS) in the Experimental Center of Exploration and Development Research Institute of Henan Oilfield Company, Sinopec. The experiment was performed on Agilent 5973 N/US55142165 GC-MS instrument equipped with an SE-54 capillary column (30 m × 0.25 mm × 0.5 μm). The injector temperature for gas chromatography (GC) analysis was 300 °C and helium was used as the carrier gas at a flow rate of 1.0 mL/min. The initial temperature of the test program was 80 °C and was held constant for 1 min. Then the temperature was raised to 310 °C at a rate of 3 °C/min and again held constant for 20 min. The mass spectrometry (MS) was operated in electron ionization (EI+) mode with an ionization energy of 70 eV and an ion source temperature of 200 °C. Data were obtained by full scan and ion selection at the same time.

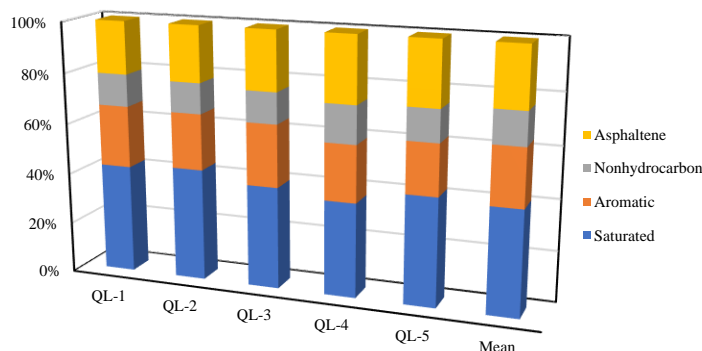


Figure 8. Group components in bitumen samples from Qinglong paleo-oil reservoir (Data from [40]).

4. Result

Aromatic hydrocarbons are composed of hundreds of compounds and contain rich geochemical information. A total of 124 aromatic compounds were identified by GC-MS analysis in bitumen samples from Qinglong paleo-oil reservoir (Figure 9). It mainly consists of phenanthrene series (m/z 178, 192, 206, 220, 234), dibenzothiophene series (m/z 184, 198, 212), fluoranthene series (m/z 202, 216) and chrysene series (m/z 228, 242, 252). There is also a small amount of fluorene series (m/z 166, 180, 194), naphthalene series (m/z 128, 142, 156, 170, 184, 198), dibenzofuran series (m/z 168, 182, 196), biphenyl series (m/z 154, 168, 182, 196) and triaromatic steroid series (m/z 231, 245).

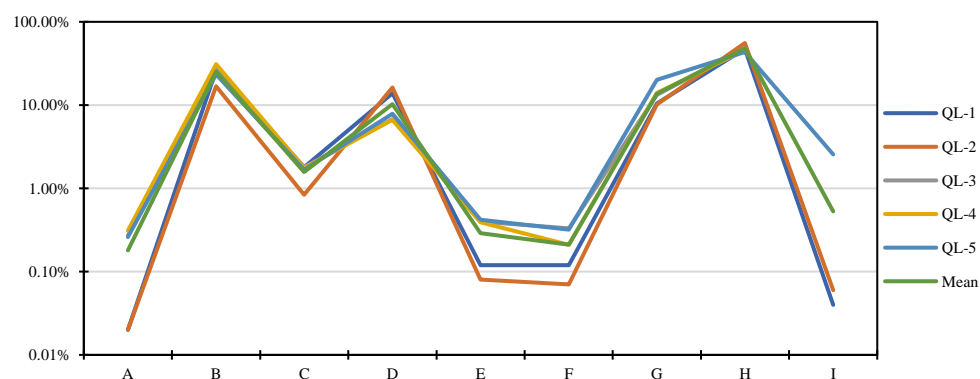


Figure 9. Composition of aromatic compounds in bitumen samples from Qinglong paleo-oil reservoir.

Note: A = naphthalene series; B = phenanthrene series; C = fluorene series; D = dibenzothiophene series; E = dibenzofuran series; F = biphenyl series; G = fluoranthene series; H = chrysene series; I = triaromatic steroid series

Compared with saturated hydrocarbons, aromatic compounds have a wider range of chemical kinetics [46], which can be better used to indicate maturity, trace the source of parent materials, judge the sedimentary environment, and discuss the TSR reaction. It is helpful to further study the characteristics and evolution of paleo-oil reservoir and its significance to antimony mineralization.

5. Discussion

5.1. Maturity of bitumen

5.1.1 Naphthalene series compounds

Naphthalene series compounds are one of the most common organic compounds in aromatic fractions of source rocks and crude oils, which can reflect the information of the source of organic matter, thermal evolution, and sedimentary environment. The relative

contents of naphthalene series compounds in bitumen samples from Qinglong paleo-oil reservoir is low, ranging from 0.02% to 0.31%, with an average of 0.18%. Naphthalene (N) and methylnaphthalene (MN) were detected in all five samples, ethylnaphthalene (EN) and dimethylnaphthalene (DMN) were detected in sample QL-3, and trimethylnaphthalene (TMN) was detected in samples QL-1 and QL-2. Due to the thermal effect, $\alpha\alpha$ configurations with higher spatial tension (e.g., 1,5-DMN) will rearrange into more stable $\beta\beta$ configurations (e.g., 2,6-DMN, 2,7-DMN). Therefore, the relative abundance of isomers can be used to evaluate the maturity of organic matter [47].

Parameters such as dimethylnaphthalene ratio (DNR) and its equivalent vitrinite reflectance (R_{c1}), trimethylnaphthalene ratio (TNR) and its equivalent vitrinite reflectance (R_{c2}) are often used to characterize the maturity of organic matter [48–49]. As dimethylnaphthalene and trimethylnaphthalene were not detected in some samples, these indexes were of poor significance to indicate the maturity of the bitumen from Qinglong paleo-oil reservoir (Table 1). In addition, the trimethylnaphthalene index (TMNr) and tetramethylnaphthalene index (TeMNR) increase gradually with the evolution of organic matter, which can be used to characterize the maturity of crude oil and source rock, and are more sensitive. In general, Both TMNr and TeMNR values are >0.5 in high mature crude oil and source rock, $0.4\text{--}0.6$ in mature crude oil and source rock, $0.3\text{--}0.5$ in low mature crude oil, and <0.4 in immature to low mature source rock [50]. Tetramethylnaphthalene (TeMN) was not detected in the bitumen samples from Qinglong paleo-oil reservoir, and the calculated TMNr value ranged from 0.66 to 0.67 (Table 1), indicating a high degree of thermal evolution.

Table 1. The maturity parameters of aromatic compounds in bitumen samples from Qinglong paleo-oil reservoir.

Sample ID	QL-1	QL-2	QL-3	QL-4	QL-5	Mean
DNR	1.64	10.00	3.74	-	-	5.13
R_{c1}	0.64	1.39	0.83	-	-	0.95
TNR	1.17	1.16	-	-	-	1.16
R_{c2}	1.10	1.10	-	-	-	1.10
TMNr	0.67	0.66	-	-	-	0.66
MPI_1	52.04	50.26	32.81	26.22	19.30	36.13
MPI_2	6.25	6.35	4.02	3.28	0.08	4.00
MPI_3	3.50	3.36	2.29	1.79	2.70	2.73
MPR	4.66	4.95	3.08	2.42	0.52	3.12
F_1	0.78	0.77	0.70	0.64	0.73	0.72
F_2	0.47	0.49	0.43	0.40	0.02	0.36
MDR	26.23	24.14	14.45	11.69	15.48	18.40
R_{c3}	1.11	0.77	17.16	29.54	17.49	13.21
R_{c4}	1.21	0.46	1.88	40.72	22.11	13.28
a	0.60	0.61	-	-	0.67	0.63
b	0.08	1.09	0.67	0.48	0.82	0.63
c	0.99	-	181.03	138.47	473.36	198.46
d	1.03	-	184.64	141.57	481.68	202.23
e	0.08	-	121.71	67.13	385.88	143.70
R_b	2.10	2.40	2.43	2.46	2.51	2.38

Note: $DNR = [(2,6\text{-DMN} + 2,7\text{-DMN})/1,5\text{-DMN}]$; $R_{c1} = 0.09 DNR + 0.49$; $TNR = [(1,3,7\text{-TMN} + 2,3,6\text{-TMN})/(1,3,5\text{-TMN} + 1,3,6\text{-TMN} + 1,4,6\text{-TMN})]$; $R_{c2} = 0.6 TNR + 0.4$; $TMNr = 2,3,6\text{-TMN} / (2,3,6 + 1,2,5\text{-TMN})$; $MPI_1 = 1.5 \cdot (3\text{-MP} + 2\text{-MP}) / (P + 9\text{-MP} + 1\text{-MP})$; $MPI_2 = 3 \cdot (2\text{-MP}) / (P + 9\text{-MP} + 1\text{-MP})$; $MPI_3 = (3\text{-MP}) / (P + 9\text{-MP} + 1\text{-MP})$

$(MP+2-MP)/(9-MP+1-MP)$; $TeMN_r = 1,3,6,7\text{-TeMN} / (1,3,6,7 + 1,2,5,7)\text{-TeMN}$; $F_1 = (3-MP+2-MP)/(1-MP+2-MP + 3-MP+9-MP)$; $F_2 = 2-MP/(1-MP+2-MP + 3-MP+9-MP)$; $MPR = 2-MP/1-MP$; $MDR = 4-MDBT/1-MDBT$; $R_{c3} (\%) = 0.14 \times (4,6\text{-DMDBT}/1,4\text{-DMDBT}) + 0.57$; $R_{c4} (\%) = 0.35 \times (2,4\text{-DMDBT}/1,4\text{-DMDBT}) + 0.46$; $a = C_{28}TAS-20S/(20R+20S)$; $b = \text{benzofluoranthrene}/\text{benzo[e]pyrene}$; $c = \text{benzo[e]pyrene}/\text{perylene}$; $d = (\text{benzo[e]pyrene} + \text{benzo[a]pyrene})/\text{perylene}$; $e = \text{benzofluoranthrene}/\text{perylene}$;
 R_b quoted from [40].

5.1.2. Phenanthrene series compounds

Phenanthrene series compounds are important components of aromatic hydrocarbon fractions, belonging to tricyclic aromatic hydrocarbons, which have been detected in source rocks, coal, and crude oil in various sedimentary environments. Many phenanthrene series compounds, including phenanthrene (P), anthracene, methylphenanthrene (MP), ethylphenanthrene (EP), dimethylphenanthrene (DMP), trimethylphenanthrene (TMP), and retene (Re) were detected in the bitumen samples from Qinglong paleo-oil reservoir. During the thermal evolution of organic matter, the methylation, methyl rearrangement and demethylation of phenanthrene series compounds were mainly controlled by thermodynamics, and migrated from thermodynamically unstable α substituents to more stable β sites with the increase of thermal evolution degree [51]. With the increase of thermal evolution, the relative contents of 2-MP and 3-MP with good thermal stability will increase, while the relative contents of 1-MP and 9-MP with poor thermal stability will decrease. Therefore, the methylphenanthrene index (MPI) [52] and the methylphenanthrene ratio (MPR) [53] are often used to study the maturity of source rocks and crude oils, and the values of these two parameters increase with the increase of maturity. The calculated results showed that the values of MPI₁, MPI₂, MPI₃ and MPR were 19.30~52.04 (average 36.13), 0.08~6.35 (average 4.00), 1.79~3.50 (average 2.73), 0.52~4.95 (average 3.12), respectively.

In addition, some other maturity parameters of phenanthrene, such as methylphenanthrene distribution fraction (MPDF), namely F_1 and F_2 , were also proposed by some scholars [54], which had a good indicator effect on samples at various maturity stages and could distinguish mature oil from highly mature oil better than MPI parameters [51]. In general, $F_1 < 0.4$ and $F_2 < 0.27$ in low maturity stage, F_1 is 0.40~0.55 and F_2 is 0.27~0.35 in maturity stage, $F_1 > 0.55$ and $F_2 > 0.35$ in over maturity stage [55]). In this study, MPI₁ showed a good positive correlation with MPI₂, MPI₃ and MPR, indicating that these maturity indicators of methylphenanthrene can effectively indicate the maturity of bitumen from Qinglong paleo-oil reservoir (Figure 10). The F_1 and F_2 values of bitumen samples range from 0.64 to 0.78 (average 0.72) and from 0.02 to 0.49 (average 0.36), respectively, suggesting that the paleo-oil reservoir is in the over-mature stage (Figure 10).

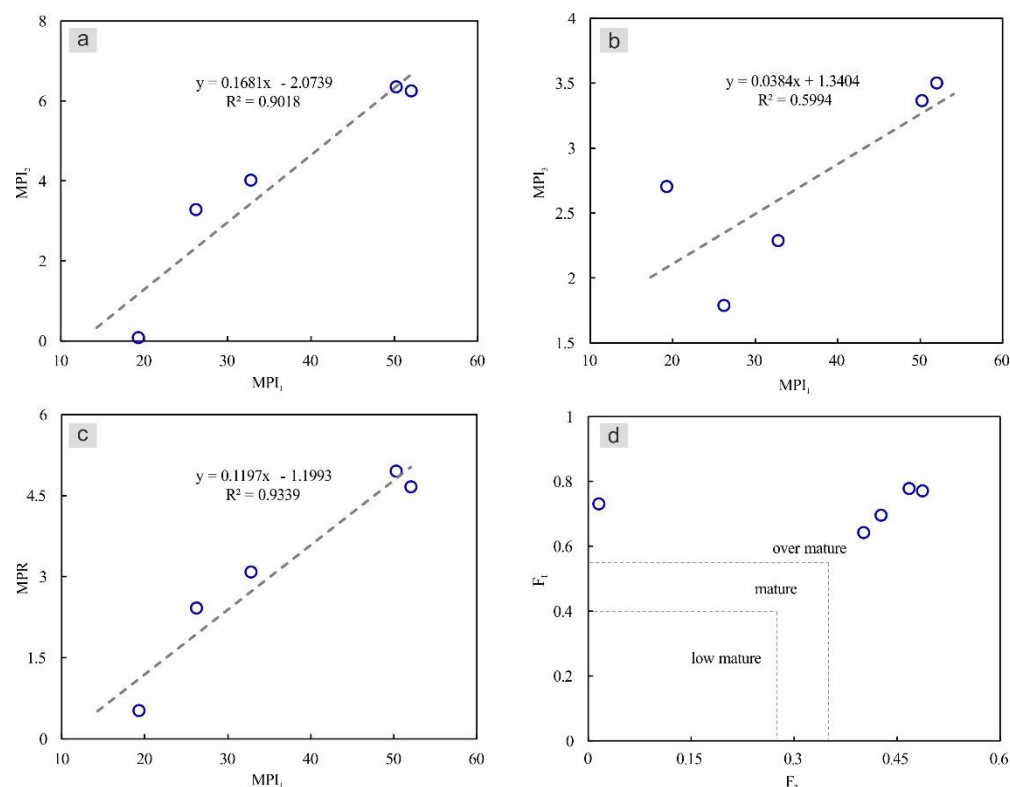


Figure 10. Correlation diagram of maturity parameters of alkyl phenanthrene in bitumen from Qinglong paleo-oil reservoir.

5.1.3 Dibenzothiophene series compounds

Dibenzothiophene (MDBT) has high thermal stability and resistance to microbial degradation, showing high and continuous sensitivity to thermal stress, and is found in crude oils and strata of all geological ages [56]. With the thermal evolution of organic matter, the relative contents of 4,6-dimethyldibenzothiophene (4,6-DMDBT) and 2,4-dimethyldibenzothiophene (2,4-DMDBT) increased, while the relative contents of 1,4-dimethyldibenzothiophene (1,4-DMDBT) decreased [57]. Accordingly, the equivalent vitrinite reflectance parameters Rc_3 and Rc_4 of dibenzothiophene were established [58]. The results of this study show that Rc_3 and Rc_4 vary widely and are of poor significance for indicating the thermal evolution degree of the paleo-oil reservoir (Table 2). In addition, the methyl-dibenzothiophene parameter (MDR) is commonly used to indicate maturity. The MDR parameter increases slightly with the increase of maturity when R_o is 0.53%-1.1%, but increases rapidly with the increase of maturity when $R_o > 1.1\%$, and the MDR value can even reach more than 30 [59]. Therefore, MDR parameters show great potential in maturity assessment of higher mature samples. In this study, the MDR values of the paleo-oil reservoir bitumen are relatively high, ranging from 11.69 to 26.23, with an average of 18.40 (Table 1), indicating a high degree of thermal evolution.

5.1.4 Other aromatic compounds

Triaromatic steranes (TAS) are the aromatization products of monaryl steranes after heating. The content of TAS in samples increases with maturity, and TAS has strong biodegradation resistance. Previous studies have shown that the $C_{28}TAS-20S/(20R+20S)$ value can be used for maturity evaluation [60]. TAS was detected in three samples in this study, and the $C_{28}TAS-20S/(20R+20S)$ values were 0.60-0.67 (average 0.63), significantly higher than those of mature source rocks (0.48-0.59, average 0.56) [60], indicating high maturity.

Benzofluoranthene and benzo[e]pyrene is both 5-ring dense aromatic hydrocarbons, and the latter is more stable. With the increase of maturity, the ratio of benzofluoranthene/benzo[e]pyrene decreases, so the ratio can be used as an indicator of maturity [50]. In addition, the ratios of benzo[e]pyrene/perylene, (benzo[e]pyrene + benzo[a]pyrene)/perylene and benzofluoranthene/perylene are also used to study the maturity of oil

source rocks, and they reach their peak values when the organic matter generates large amounts of hydrocarbons [61]. In this study, the values of benzo[e]pyrene/perylene, (benzo[e]pyrene + benzo[a]pyrene)/perylene and benzo fluoranthene/perylene are 198.46, 202.23 and 143.70, respectively, which were poor indicators of maturity. Benzo fluoranthene/benzo[e]pyrene values are relatively low, ranging from 0.08 to 1.09 (average 0.63), suggesting a high degree of thermal evolution.

In summary, these parameters, such as DNR, R_{c1} , TNR, R_{c2} , R_{c3} , R_{c4} , benzo[e]pyrene/perylene, (benzo[e]pyrene + benzo[a]pyrene)/perylene and benzofluoranthene/perylene, are not suitable for evaluating the thermal evolution of the Qinglong paleo-oil reservoir, which may be related to high maturity and biodegradation. Parameters such as TMNr, MPI, MPDF (F_1 and F_2), MDR, $C_{28}TAS-20S/(20R+20S)$, and benzofluoranthene/benzo[e]pyrene indicate high maturity, which is consistent with the measured bitumen reflectance (Rb) values (mean 2.38, over-mature stage) [40].

5.2 Parent material of paleo-oil reservoir and the sedimentary environment of source rocks

5.2.1 Parent material of paleo-oil reservoir

Previous studies have shown that there is a close relationship between the parent material source of crude oil and the relative content of some aromatic compounds. Aromatic compounds such as naphthalene series (1,2,5-trimethylnaphthalene (1,2,5-TMN), 1,2,5,6-tetramethylnaphthalene (1,2,5,6-TeMN), benzofluoranthene, fluoranthene, retene, cadalene, pyrene, anthracene, perylene and biphenyl, etc., are biomarkers reflecting terrigenous organic matter input [46,62–65]. Compounds chrysene and phenanthrene series are closely related to the input of lower aquatic organisms [62]. The ratio of (1,2,5-TMN)/(1,3,6-TMN) is used to distinguish marine and continental crude oil, and this ratio <0.3 in marine crude oil >0.3 in terrestrial crude oil and 0.71–1.48 in oil derived coals [64].

These aromatic compounds such as naphthalene series, benzofluoranthene, fluoranthene, pyrene, anthracene, retene, perylene and biphenyl were detected in the bitumen samples, but most of them had low content (Figure 1), indicating that the Qinglong paleo-oil reservoir had a small amount of higher plant input. At the same time, the concentrations of phenanthrene and chrysene in aromatic compounds were both very high, ranging from 16.86–30.90% (average 24.79%) and 12.29–23.28% (average 18.53%), respectively (Table 1), indicating that the parent material of the paleo-oil reservoir was mainly from low aquatic organisms. This is consistent with a mixed source dominated by lower organisms as revealed by the Pr/C17–pH/C18 plot [40].

5.2.2 Sedimentary environment of source rock

Some studies have detected retene in the fraction produced by pyrolysis of green algae and cyanobacteria, and it is believed that the formation of retene is related to the reducing environment [66]. The triaromatic steroid series compounds are thought to be associated with salt water environment or low maturity of organic matter [67], and the relative content of the triaromatic steroid series in marine crude oil and oil derived coals is generally $<3\%$ [46]. In addition, the formation of perylene requires a strongly reduced deposition environment [68]. A certain amount of retene, triaromatic steroid series and perylene were detected in this study, which indicated that the source rock of the paleo-oil reservoir was formed in a relatively reductive sedimentary environment.

Phenanthrene (P) compound in aromatic hydrocarbons is the product of diagenetic evolution of sedimentary organic matter. The ratio of pristane to phytane (Pr/Ph) in alkanes can be a good indicator of the redox environment, while dibenzothiophene (DBT) appears in the depositional environment with strong reducing ability, abundant reduced sulfur, and less iron ions. Thus, Crossplot of DBT/P versus Pr/Ph was established and used to distinguish sedimentary environments [69–70]. In Pr/Ph–DBT/P binary plot (Figure 11a), the bitumen samples from Qinglong paleo-oil reservoir plot into the field of sulfur-poor lacustrine environment.

Previous studies have shown that the high content of fluorene (F) series compounds appears in source rocks formed in terrestrial freshwater to slightly saline lake facies, while the high content of dibenzofuran (DBF) series is found in marsh coal. In addition, the

source rocks formed in saltwater lake and marine facies have high content of dibenzothiophene (DBT) series [71–72]. The relative composition characteristics of the three series of compounds are often used to characterize the changes of sedimentary environment [73–74]. The transition environments between oxidation and reduction are more easily distinguished by the Crossplot of $\Sigma\text{DBT}/\Sigma(\text{F}+\text{DBT})$ versus $\Sigma\text{DBF}/\Sigma(\text{F}+\text{DBF})$ [75]. Furthermore, the binary plot of Pr/Ph versus DBT/DBF can effectively judge the oxidation-deoxidation environment [75].

In the ternary diagram of DBF–DBT–F (Figure 11b) and binary plot of DBT/(F+DBT)–DBF/(F+DBF) (Figure 11c), the bitumen samples from Qinglong paleo-oil reservoir are all related to the swamp environment. In the binary plot of Pr/Ph versus DBT/DBF (Figure 11d), All the studied samples plot into the field of weak oxidation to weak reduction environment, which is consistent with the above analysis.

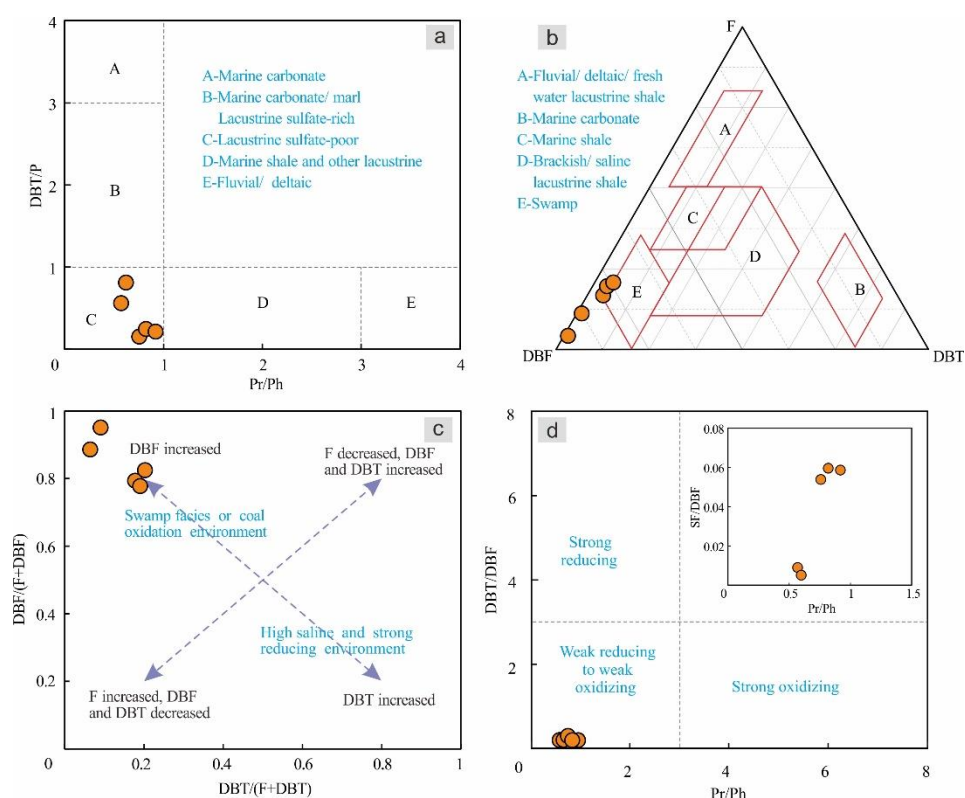


Figure 11. Discrimination diagram of sedimentary environment. (a) Crossplot of Pr/Ph versus DBT/P; (b) Ternary diagram of DBF–DBT–F; (c) Binary plot of DBT/(F+DBT) versus DBF/(F+DBF); (d) Crossplot of Pr/Ph–DBT/DBF.

In addition, dibenzothiophene series compounds are abundant in Qinglong paleo-oil reservoir, with a relative content of 6.63–16.26% (average 10.28%), which is much higher than that of lacustrine oil and coal-formed oil (average 2.5% and 3.2%, respectively), and close to that of marine facies oil (average 7.7–42.5%, average 20.6%) [61]. In a word, the comprehensive analysis shows that the source rock of Qinglong paleo-oil reservoir was formed in the marine environment of weak oxidation and weak reduction.

5.3 Source rock of Paleo-oil reservoir

The source rocks developed in the southwest Guizhou depression of Nanpanjiang Basin include Middle Devonian Huohang Formation (D_2h), Lower Carboniferous Jiusi Formation (C_1j), Middle Permian Liangshan Formation (P_2l) and Upper Permian Longtan Formation (P_3l), which are also the target beds for shale gas exploration in this area (Figure 2) [76]. Previous studies have shown that the main source rocks in the Nanpanjiang Depression are black mudstones deposited in the middle Devonian basin facies, such as Luofu Formation (D_2l) and Nabiao Formation (D_2n), which are characterized by huge

thickness, high organic carbon content and mainly sapropelic organic matter; In addition, the lithology of Carboniferous, Permian and Triassic is mainly carbonate rocks, followed by marl and calcareous mudstone, so the distribution of effective source rocks is limited [77–78].

The study shows that there are many reefs limestone paleo-oil reservoirs (D₂-P₃) and some high N₂ gas reservoirs (such as Shuang1 well and Yang1 well) distributed in the Nanpanjiang Depression (Figure 1), which are all derived from the Devonian source rocks; Paleo-oil reservoir bitumen is considered as the pyrobitumen produced in the process of oil cracking into gas under the action of high temperature and pressure, and high N₂ natural gas is derived from the gas generated by the kerogen cracking of the Middle Devonian source rocks [79–81]. The physical characteristics and geochemical analysis of bitumen in this study show that it is also the pyrobitumen formed by thermal cracking of early paleo-oil reservoir due to the rise of paleo-geothermal temperature [37]. The study of saturated hydrocarbon biomarkers, carbon isotopes and rare earth elements shows that Qinglong paleo-oil reservoir originated from Devonian source rocks, just like other paleo-oil reservoirs and natural gas reservoirs in the Nanpanjiang basin [40].

5.4 Indication of the TSR reaction

Thermochemical sulfate reduction (TSR), refers to the chemical reaction of sulfate with organic matter or hydrocarbons to reduce sulfate minerals and generate hydrogen sulfide (H₂S) and carbon dioxide (CO₂). The concept of TSR was first proposed by Orr (1974) to explain the presence of large amounts of H₂S in natural gas in the Big Horn Basin [82]. In fact, oil and gas reservoirs with high H₂S content are widely distributed around the world and reach the scale of industrial oil and gas flows [83–84]. These reservoirs are mainly located in Canada [85–87], the United States [82,88] and Mexico in North America, Iran [89], Iraq, Saudi Arabia [90] and the United Arab Emirates [91] in the Middle East, the Amu Darya River, North Caspian Sea, Volga-Urals, Siberia and the Timan-Pechora in the former Soviet Union [85], Croatia [92], Germany and France in Europe, China's Sichuan and Tarim Basin [93–94] and India [85] in Asia. The buried depth of these reservoirs ranges from 500 m to 6000 m, and the reservoir strata are Sinian to Tertiary [83–84]. Among them, the South Texas gas reservoir has the highest H₂S content of 98%; The H₂S content in the world-class Lacq gas field in France and the Puguang and Dukouhe giant gas fields in Sichuan Basin, China, all exceeded 15% [95–96].

As a reducing agent, the organic matter of oil and gas produces a large amount of reduced sulfur through TSR reaction, which is the only way to form high concentration H₂S oil and gas reservoirs. TSR reaction is also an important formation mechanism of reduced sulfur in many metal deposits [6,38,97–98]. TSR total reaction equation is as follows:

$$\text{Hydrocarbons} + \text{SO}_4^{2-} \rightarrow \text{altered hydrocarbons} + \text{solid bitumen} + \text{HCO}_3^- (\text{CO}_2) + \text{H}_2\text{S} (\text{HS}^-) + \text{heat} \pm \text{H}_2\text{O} [99].$$

TSR is considered to be an autocatalytic process, and thiols and other sulfides are intermediate transition products. The specific reaction process can be roughly divided into 3 steps (Figure 12) [100].

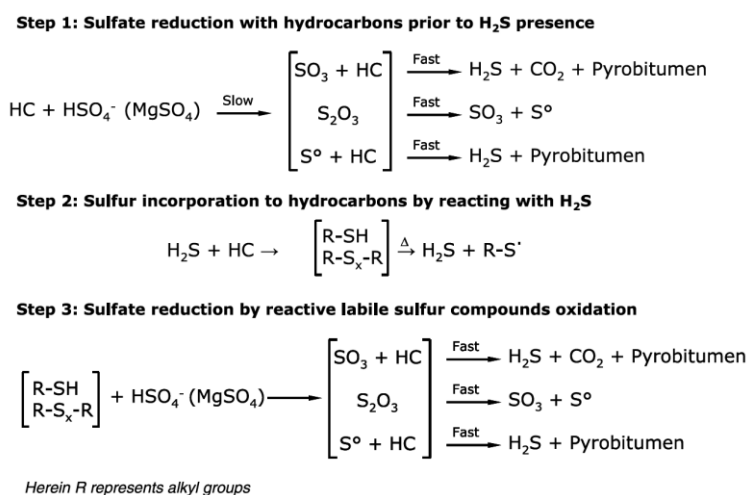


Figure 12. TSR reaction mechanism (after [100]).

Many studies have shown that H₂S produced in the TSR reaction process reacts with hydrocarbon compounds to form new sulfur-containing compounds, such as thiophene (TP), tetrahydrothiophene (THTP), benzothiophene (BP), dibenzothiophene (DBT), thiadiazole (TA), etc. [101–106], which leads to an increase in sulfur content, a decrease in saturated hydrocarbon/aromatic ratio, and an increase in non-hydrocarbon and asphaltene content of crude oil [107]. Wang et al. (2013) believed that TSR reaction occurred in Majiang large paleo-oil reservoir in Guizhou Province, and in this process, biphenyl (BP) was transformed into dibenzothiophene (DBT), methylbiphenyl (MBP) was transformed into methylthiobiphenyl (MTBP), and dimethylbiphenyl (DMBP) was transformed into dimethylthiobiphenyl (DMTBP) [108].

The formation order of sulfur compounds is thiophene, tetrahydrothiophene, benzothiophene, dibenzothiophene and thiadiazole, which is related to its own stability [109]. Tetrahydrothiophene and benzothiophene compounds with poor thermal stability were formed earlier and faster in TSR reaction, while dibenzothiophene and thiadiazole compounds with relatively high stability were formed more slowly, and it was difficult to take further reaction once formed. Although a small amount of dibenzothiophene and thiadiazole can be inherited from source rocks, TSR can produce a large amount of dibenzothiophene and thiadiazole at a high degree of modification, which is much more than that from kerogen sources. Therefore, higher concentrations of dibenzothiophene and thiadiazole are considered to be the marker compounds for TSR reaction [104–105].

In general, dibenzothiophene series compounds are not very abundant in the aromatic components of source rocks or crude oils. For example, its relative content is 1.29% on average in the source rocks from the Jurassic Haifanggou Formation in Niuyingzi Depression of Lingyuan-Ningcheng Basin [46], < 2.5% in the Paleogene source rock in Miaoxibe Sag of Bohai Sea area [110], 2.67% on average in the crude oil from Chi'an Oilfield in Gaoyou Sag [111], and < 4% in Light Oils from Xihu Sag in East China Sea Basin [112].

The bitumen samples of Qinglong paleo-oil reservoir contain abundant dibenzothiophene series compounds, the relative content ranges from 6.63 to 16.26%, with an average of 10.28% (Figure 13). Dibenzothiophene (DBT) and methylthiobiphenyl (MTBP) were the main compounds in dibenzothiophene series, and their relative contents are 1.09-6.63% (average 3.37%) and 1.95-7.53 (average 4.08%), respectively (Figure 14). A small amount of dimethylthiobiphenyl (DMTBP) is also included, with a relative content of 0.06-0.28% and an average of 0.18%. While, the biphenyl series (including BP, MBP and DMBP) in the ancient reservoir is very small, with the relative content ranging from 0.07 to 0.33%, with an average of 0.21% (Figure 13,14). Therefore, we believe that Qinglong paleo-oil reservoir underwent a certain degree of TSR alternation, during which some biphenyl series compounds were converted into dibenzothiophene series compounds, and a large amount of H₂S was generated.

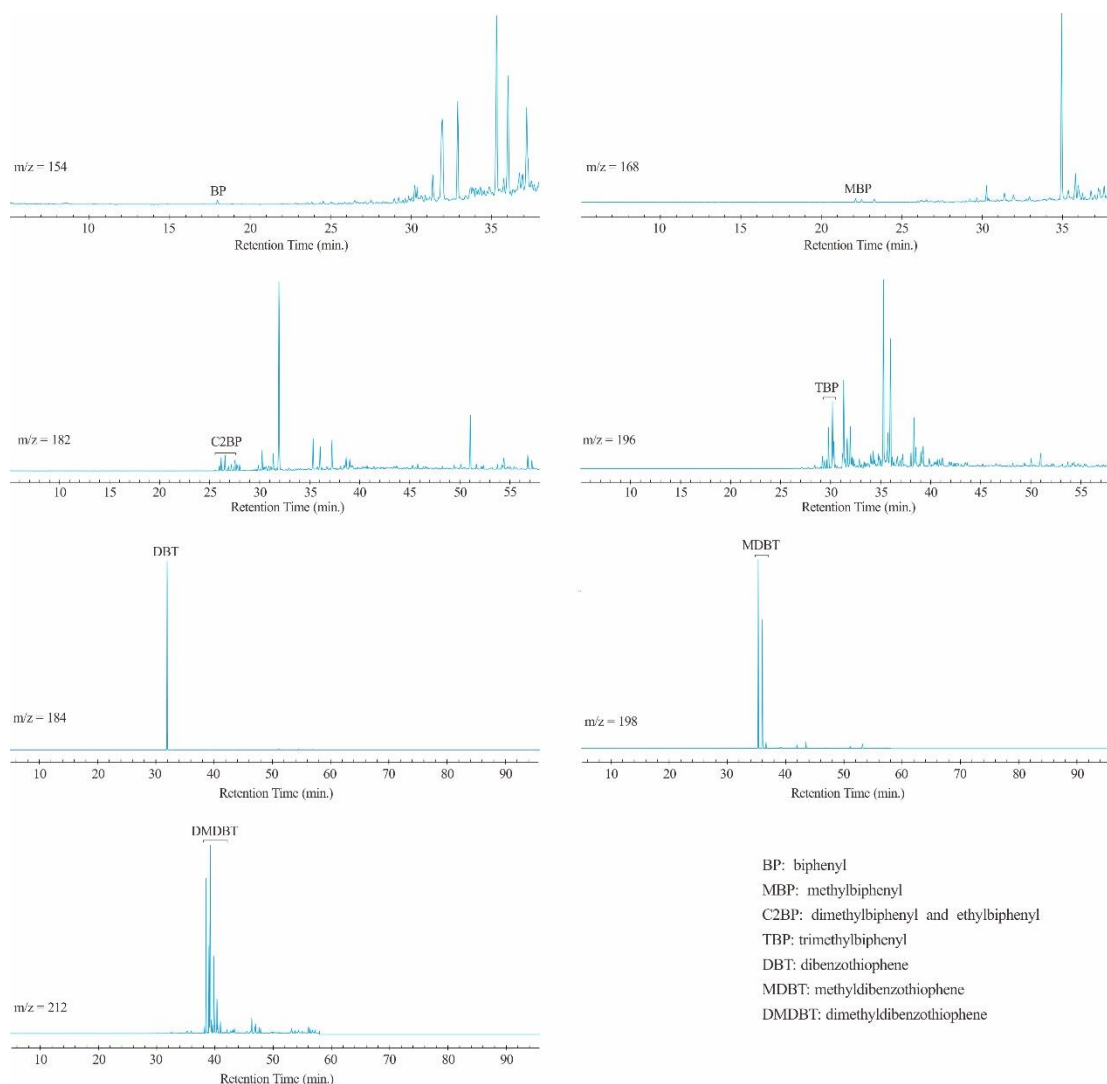


Figure 13. Mass chromatograms of the biphenyl series and dibenzothiophene series (QL-1).

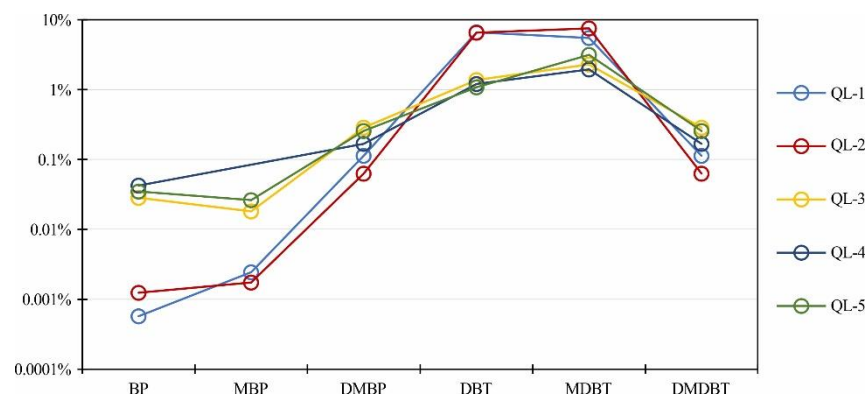


Figure 14. Relative percentage of the biphenyl series and dibenzothiophene series.

5.5 Genetic relationship between paleo-oil reservoir and antimony deposits

5.5.1 Spatial-temporal relationship between hydrocarbon accumulation and antimony mineralization

The spatial relationship between paleo-oil reservoir and Qinglong antimony ore field is very close (Figure 3). The antimony body is close to the core of the Dachang anticline and is distributed in the Upper Permian "Dachang layer" between the Huyujing fault and Qingshanzhen fault, which is obviously controlled by the NE trending fault. The paleo-oil reservoir is located in the northwest wing of Dachang anticline, and its reservoirs are

mainly Emeishan basalt, “Dachang layer” and Maokou Formation. The paleo-oil reservoir is closely associated with the antimony deposit, which is about 2.5 km apart in plane, and the vertical hosting horizon is also consistent.

According to the parameters of strata, lithology and geochemistry, the Basin Model software is used to simulate the burial history, thermal history, and maturation history of paleo-oil reservoir (Figure 15). The exponential compaction model, instantaneous heat flow model and Easy Ro model are used to simulate the burial history, thermal history and maturation history, respectively. The results show that rapid burial occurred during the Permian to Early Jurassic, during which the paleo-oil reservoir strata (Middle Permian) were rapidly buried below 5500 m; Although slow uplift occurred in the late Early Jurassic to Early Cretaceous, the buried depth of the paleo-oil reservoir strata was always below 4000 m; Rapid uplift occurred since the Late Cretaceous, and the paleo-reservoir strata were exposed to the surface and eroded by weathering since the Eocene. The previous bitumen Re-Os isotopic chronology indicates that the age of oil generation peak of the Devonian source rock is 254 Ma (early Late Permian) [38]. The basin simulation in this study indicates that the paleo-oil reservoir formed in the early to middle Triassic and evolved into gas reservoir (mainly bitumen + methane) at the end of the late Triassic. The paleo-oil reservoir bitumen had experienced high temperature above 200 °C and has a high degree of thermal evolution, which is consistent with the aromatic maturity parameters and the measured R_o data [40]. The Sm-Nd isotopic isochron ages of calcite and fluorite in Qinglong antimony ore field indicate that the metallogenic epoch is late Jurassic (142-148 Ma) [24,29]. Therefore, in terms of time relationship, oil and gas accumulation was earlier than metal antimony mineralization, and the paleo-oil reservoir had already been thermally cracked to become the paleo-gas reservoir.

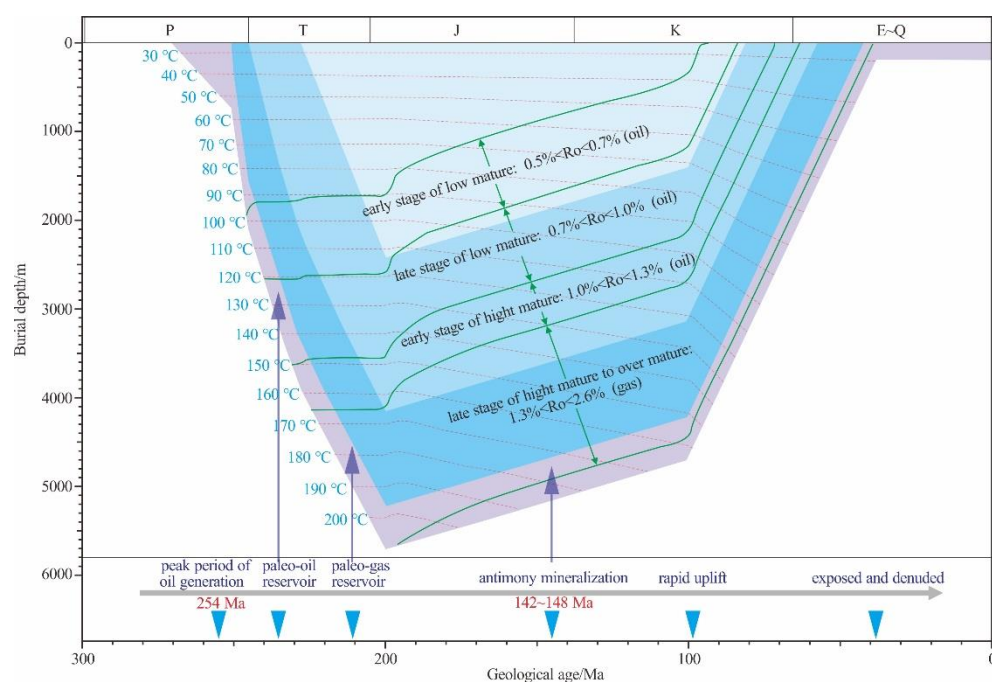


Figure 15. Simulation results of burial history, thermal history and maturation history of Qinglong Paleo-oil reservoir show the time relationship between hydrocarbon evolution and antimony mineralization.

5.5.2 The role of paleo-oil reservoir in antimony mineralization

In terms of material connection, although the low Sb content of paleo-oil reservoir bitumen suggests that the hydrocarbon substances failed to contribute metal Sb to mineralization [40]. However, the composition of organic inclusions in the deposit is similar to that of natural gas reservoirs in Nanpanjiang Basin. In addition, the paleo-oil reservoir and antimony deposit have similar S isotope characteristics [40]. Therefore, we believe that the paleo-gas reservoir formed by the evolution of paleo-oil reservoir participated in

Sb mineralization, that is, hydrocarbon organic matter acted as reducing agent and transformed SO_4^{2-} in oilfield brine into H_2S through TSR, providing reduced sulfur and creating environmental conditions for mineralization. Since the gaseous hydrocarbon rather than liquid hydrocarbon is involved in antimony mineralization, the phenomenon of mineral paragenesis of solid bitumen and stibnite is not found in the ore, but organic gas components are common in the ore inclusions.

Some scholars hold different views that the Qinglong antimony deposit S originated from magma [22,27]. However, 2D seismic data reveal that there is no hidden rock mass in Nanpanjiang Basin [42,45]. The hidden magmatic rock mass previously inferred from gravity and aeromagnetic anomalies is actually a palaeohigh above the basement, which controls the distribution of Au-Sb deposits [45].

It has been confirmed that Sb originated from “Dachang layer”, and the ore-forming fluid is mainly basin fluid [40]. Therefore, on the basis of previous studies, we proposed a model diagram of the involvement of gaseous hydrocarbon organic matter formed by the pyrolysis of ancient oil reservoir in Sb mineralization (Figure 16).

With the rapid burial of the strata, the Devonian source rock matured in the early Late Permian and a large amount of oil was generated. A large number of hydrocarbon fluids migrated upward and gradually accumulated under the shielding effect of tuff in the third member of “Dachang layer”, and then the paleo-oil reservoir was formed during the early to middle Triassic.

After that, the heated basin fluid continuously extracted metal Sb in “Dachang layer”, and gradually formed Sb-rich ore-forming fluid. On the other hand, with burial heating, the paleo-oil reservoir gradually cracked, forming the paleo-gas reservoir and a large amount of solid bitumen at the end of the late Triassic, and generating a large amount of H_2S through TSR reaction.

In the late Jurassic, Sb-rich ore-forming fluids gradually accumulated in the Dachang palaeohigh. Due to the change of physical and chemical conditions, the metal Sb combines with H_2S and precipitates to form the deposit at the appropriate position.

Since the late Cretaceous, with the rapid uplift of the crust, the antimony deposits were lifted to the near surface position, while the paleo-gas reservoir was destroyed by denudation and a large amount of solid bitumen remained.

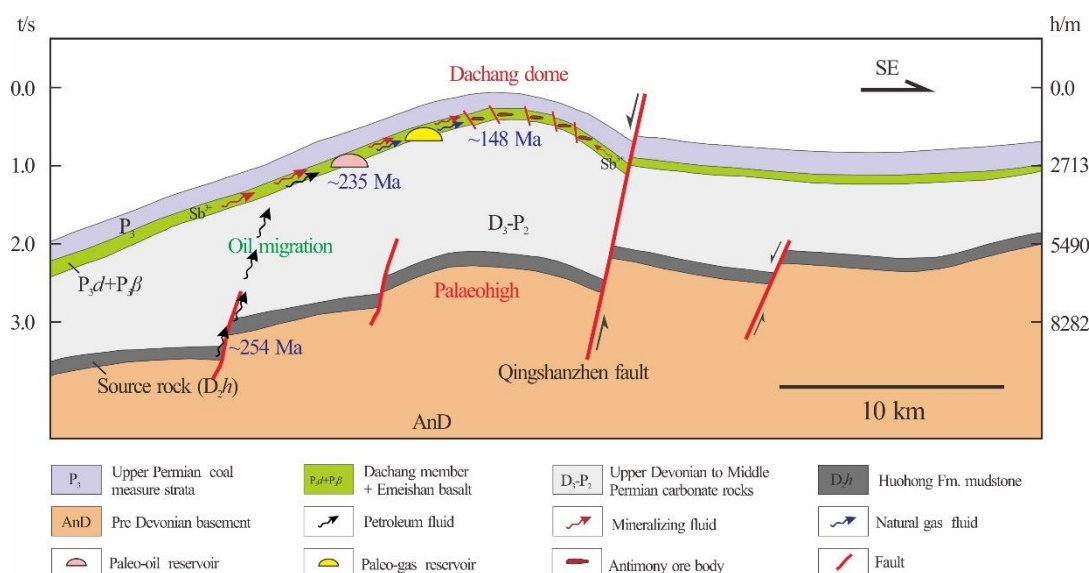


Figure 16. Schematic metallogenic model for the Qinglong antimony deposit, showing the genetic relationship between oil and gas accumulation and antimony mineralisation. The stratum, structure and depth of the figure are based on 2D seismic profile interpretation, which is NW-SE striking and adjacent to the northern area of Figure 2, modified from [38,40].

6. Conclusion

Various aromatic compounds have been detected in Qinglong paleoreservoir bitumen, including abundant phenanthrene series, dibenzothiophene series, fluoranthene series, chrysene series, and a small number of fluorene series, naphthalene series, dibenzofuran series, biphenyl series, triaromatic steroid series.

Aromatic compounds and their related parameters indicate that the paleo-reservoir is in over mature level, and the parent material of the paleo-oil reservoir was mainly low aquatic organisms, mixed with a small amount of higher plant. The paleo-oil reservoir was derived from the Devonian source rock, which was formed in the marine environment of weak oxidation and weak reduction.

Abundant dibenzothiophene series and less biphenyl series were detected, indicating that the paleo-oil reservoir underwent a certain degree of TSR reaction. We believe that the paleo-gas reservoir formed by the evolution of paleo-oil reservoir participated in antimony mineralization, that is, hydrocarbon organic matter acted as reducing agent and transformed SO_4^{2-} in oilfield brine into H_2S through TSR, providing reduced sulfur and creating environmental conditions for mineralization.

Author Contributions: Conceptualization, Y.H.; investigation, Y.H. and D.W.; data curation, Y.C. and S.X.; writing—original draft preparation, Y.C.; writing—review and editing, Y.C., Y.H. and S.X.; supervision, Y.H.; funding acquisition, Y.H. All authors have read and agreed to the published version of the manuscript.

Funding: This research was jointly supported by the National Natural Science Foundation of China (41672073) for Yuzhao Hu.

Data Availability Statement: Not applicable.

Acknowledgments: Thanks to Professor Wang Guozhi for the invitation, Professor Chen Jun for the photos, and MPDI for the language editing service.

Conflicts of Interest: The authors declare no conflict of interest.

References

1. Liu C. Dynamics of sedimentary basin and basin reservoir (ore) forming system. *J. Earth Sci. Environ.*, **2008**, (1): 1-23. (In Chinese with English Abstract)
2. Fuchs S., Schumann D., Martin R.F., Couillard M. The extensive hydrocarbon-mediated fixation of hydrothermal gold in the Witwatersrand Basin, South Africa. *Ore Geol. Rev.*, **2021**, 138: 104313.
3. Pons M.J., Franchini M., Rainoldi A.L., Giusiano A., Cesaretti N.N., Montagna A.O., Herrington R. Base metal mobility linked to brine and hydrocarbon migration at the Huincul High in the Neuquén Basin, Argentina: Implications for the formation of sediment-hosted base metal deposits. *J. Geochem. Explor.*, **2021**, 226: 106778.
4. Boreham C.J., Sohn J.H., Cox N., Williams J., Hong Z., Kendrick M.A. Hydrogen and hydrocarbons associated with the Neoproterozoic Frog's Leg Gold Camp, Yilgarn Craton, Western Australia. *Chem. Geol.*, **2021**, 575: 120098.
5. Vinnichenko G., Hope J.M., Jarrett A.J., Williams N., Brocks J.J. Reassessment of thermal preservation of organic matter in the Paleoproterozoic McArthur River (HYC) Zn-Pb ore deposit, Australia. *Ore Geol. Rev.*, **2021**, 133: 104129.
6. Ge X., Selby D., Liu J., Chen Y., Cheng G., Shen C. Genetic relationship between hydrocarbon system evolution and Carlin-type gold mineralization: Insights from Re-Os pyrobitumen and pyrite geochronology in the Nanpanjiang Basin, South China. *Chem. Geol.*, **2021**, 559: 119953.
7. Wang G., Huang Z., Zhao F., Li N., Fu Y. The relationship between hydrocarbon accumulation and Mississippi Valley-type Pb-Zn mineralization of the Mayuan metallogenic belt, the northern Yangtze block, SW China: Evidence from ore geology and Rb-Sr isotopic dating. *Resour. Geol.*, **2020**, 70(2): 188-203.
8. Chi G., Xue C., Sun X., Lai J., Luo P., Song H., Li S., Zeng R. Formation of a giant Zn-Pb deposit from hot brines injecting into a shallow oil-gas reservoir in sandstones, Jinding, southwestern China. *Terra Nova*, **2017**, 29(5): 312-320.
9. Gu X.X., Li B.H., Dong S.Y., Xue C.J., Fu S.H. Hydrocarbon- and ore-bearing basinal fluids: a possible link between gold mineralization and hydrocarbon accumulation in the Youjiang basin, South China. *Miner. Deposita*, **2012**, 47(6): 663-682.
10. Wu Y., Zhang C., Mao J., Ouyang H., Sun J. The genetic relationship between hydrocarbon systems and Mississippi Valley-type Zn-Pb deposits along the SW margin of Sichuan Basin, China. *Int. Geol. Rev.*, **2013**, 55(8): 941-957.
11. Hulen J.B., Collister J.W. The oil-bearing, carlin-type gold deposits of Yankee Basin, Alligator Ridge District, Nevada. *Econ. Geol.*, **1999**, 94(7): 1029-1049.
12. Fallara F., Savard M.M. A structural, petrographic, and geochemical study of the Jubilee Zn-Pb deposit, Nova Scotia, Canada, and a new metallogenic model. *Econ. Geol.*, **1998**, 93(6): 757-778.

13. Gu X, Zhang Y., Li B., Xue C., Dong S., Fu S., Cheng W., Liu L., Wu C. The coupling relationship between metallization and hydrocarbon accumulation in sedimentary basins. *Earth Sci. Front.*, **2010**, 17(2): 89-111. (In Chinese with English Abstract)
14. Hu Y., Ren T. Metal deposits, oil and gas reservoirs: two brothers in sedimentary basin. *Chin. J. Nat.*, **2019**, 41(1): 48-52. (In Chinese with English Abstract)
15. Liu J., Ye J., Liu J., Tan J., Niu J. Oil accumulation and ore-formation. *Bull. Mineral., Petrol. Geochem.*, **2000**, (3): 164-171. (In Chinese with English Abstract)
16. Li R., Mao J, Zhao B., Chen B., Liu S. A review of the role of hydrocarbon fluid in the ore formation of the MVT Pb-Zn deposit. *Adv. Earth Sci.*, **2021**, 36(4): 335-345. (In Chinese with English Abstract)
17. Tu G. The relationship between coal, oil, gas, salt and metal ore formation. *Geol. Explor. Non-Ferrous Met.*, 1994, 3(1): 1-3. (In Chinese)
18. Chen G., Xu G., Wang T., Ma L, Shi L, Zheng C. The relationship between hydrocarbon accumulation and metallization and a discussion on intergrated exploration. *Earth Sci. Front.*, **2008**, (2): 200-206. (In Chinese with English Abstract)
19. Luo K., Zhou J., Feng Y., Uysal I.T., Nguyen A., Zhao J., Zhang J. In situ U-Pb Dating of calcite from the South China antimony metallogenic belt. *Iscience*, **2020**, 23(10).
20. Ding J., Zhang Y., Ma Y., Wang Y., Zhang J., Zhang T. Metallogenic characteristics and resource potential of antimony in China. *J. Geochem. Explor.*, **2021**, 230: 106834.
21. Yan J., Fu S., Liu S., Wei L., Wang T. Giant Sb metallogenic belt in South China: A product of Late Mesozoic flat-slab subduction of paleo-Pacific plate. *Ore Geol. Rev.*, **2022**, 142: 104697.
22. Chen J., Huang Z., Yang R., Du L., Liao M. Gold and antimony metallogenic relations and ore-forming process of Qinglong Sb (Au) deposit in Youjiang basin, SW China: Sulfide trace elements and sulfur isotopes. *Geosci. Front.*, **2021**, 12(2): 605-623.
23. Chen J., Yang R., Du L., Gao J., Zheng L., Huang Z. Multistage fluid sources and evolution of Qinglong Sb-(Au) deposit in northern margin of Youjiang basin, SW China: REE geochemistry and Sr-H-O isotopes of ore-related jasperoid, quartz and fluorite. *Ore Geol. Rev.*, **2020**, 127: 103851.
24. Wang D., Qin Y., Wang C., Chen Y., Gao L. Mineralization pedigree for epithermal Hg, Sb, Au deposits in Guizhou Province—taking the Dachang Sb deposit, the Zimudang Au deposit and the Luanyantang Hg deposit for examples. *Geotecton. Metallog.*, **2012**, 36(3): 20-26. (In Chinese with English Abstract)
25. Hu Y., Zhao Y., Liu L., Wang J., Li W. Study on metallogenic coupling of compound half-graben and basin fluid in the Qinglong antimony deposit. *Geotecton. Metallog.*, **2014**, 38(4): 802-812. (In Chinese with English Abstract)
26. Su W., Zhu L, Ge X, Shen N., Zhang X, Hu R. Infrared microthermometry of fluid inclusions in stibnite from the Dachang antimony deposit, Guizhou. *Acta Petrol. Sin.*, **2015**, (4): 14-20. (In Chinese with English Abstract)
27. Chen J., Yang R., Du L., Zheng L., Gao J., Lai C., Wei H., Yuan M. Mineralogy, geochemistry and fluid inclusions of the Qinglong Sb-(Au) deposit, Youjiang basin (Guizhou, SW China). *Ore Geol. Rev.*, **2018**, 92: 1-18.
28. Chen Y., Liu X., Zhang Q. A tentative discussion on the genesis of the Dachang antimony deposit, Qinglong county, Guizhou province. *Miner. Deposits*, **1984**, (3): 1-12. (In Chinese with English Abstract)
29. Peng J., Hu R., Jiang G. Samarium-Neodymium isotope system of fluorites from the Qinglong antimony deposit, Guizhou Province: Constraints on the mineralizing age and ore-forming materials' sources. *Acta Petrol. Sin.*, **2003**: 785-791. (In Chinese with English Abstract)
30. Zhu J., Fang W., Liu J., Hu Y. The REE characteristics and genetic study of Qinglong antimony deposit, Guizhou. *Contrib. Geol. Miner. Resour. Res.*, **2010**, (2): 118-123. (In Chinese with English Abstract)
31. Xiong C., Liu J., Liu S., Wang D., Yang C., Wang Z., Chen R. Study on fluid inclusion of Qinglong Dachang antimony deposit. *J. Guizhou Univ., Nat. Sci. Ed.*, **2013**, 30(6): 47-52. (In Chinese with English Abstract)
32. Chen X., Su W., Huang Y. He and Ar isotope geochemistry of ore-forming fluids for the Qinglong Sb deposit in Guizhou Province, China. *Acta Petrol. Sin.*, **2016**, 32(11): 76-84. (In Chinese with English Abstract)
33. Pan J., Wu D. Comparison of sources for the ore-forming fluids and materials for the antimony ore deposits in South and South-west of Guizhou Province, China. *Geol. Sci. Technol. Inf.*, **2017**, 36(4): 123-132. (In Chinese with English Abstract)
34. Wang H., Yi J. The relationship between the organic matter and the antimony mineralization in Dachang district, Guizhou. *Bull. Mineral., Petrol. Geochem.*, **1996**, 15(2): 84-87. (In Chinese with English Abstract)
35. Ye Z., Yi J., Hu R. Organic matter and its role in mineralization in Dachang antimony deposit, Guizhou, China. *Acta Mineral. Sin.*, **1997**, 17(3): 310-315. (In Chinese with English Abstract)
36. Liu L., Hu Y., Zhang G. Raman spectral characteristics of Qinglong antimony ore field paleo-oil reservoir bitumen and hydrocarbon inclusions. *Geol. Rev.*, **2016**, 62(4): 1010-1020. (In Chinese with English Abstract)
37. Wang P., Hu Y., Liu L., Zhang G. Geochemical characteristics and genesis of bitumen in paleo-oil reservoir in Qinglong antimony deposit, Guizhou. *J. Xi'an Shiyou Univ., Nat. Sci. Ed.*, **2016**, 31(2): 44-49, 56. (In Chinese with English Abstract)
38. Wang P., Hu Y., Liu L., Jiang X., Li C., Bartholomew C.J., Zhang G. Re-Os dating of bitumen from paleo-oil reservoir in the Qinglong antimony deposit, Guizhou Province, China and its geological significance. *Acta Geol. Sin.*, **2017**, 91(6): 2153-2163.
39. Wang P., Hu Y., Liu L., Zhang G. REE geochemical characteristics and significance for bitumen in paleo-oil reservoir in Qinglong antimony deposit, Guizhou Province, China. *Acta Mineral. Sin.*, **2017**, 37(1): 106-113. (In Chinese with English Abstract)
40. Cheng Y., Hu Y., Wang D., Wang P., Li P., Wang X. Oil-source rock analysis and metallogenic significance of the palaeo-oil reservoir in the Qinglong antimony deposit, South China. *Ore Geol. Rev.*, **2021**, 137: 104281.
41. Hu R., Fu S., Huang Y., Zhou M., Fu S., Zhao C., Wang Y., Bi X., Xiao J. The giant South China Mesozoic low-temperature metallogenic domain: Reviews and a new geodynamic model. *J. Asian Earth Sci.*, **2017**, 137: 9-34.

42. Hu Y., Liu W., Zhang G., Guan S., Lu Y., Li P., Zheng S., Fan H., Betts P.G. Seismic reflection profiles reveal the ore-controlling structures of Carlin-style gold deposits in Lannigou gold fields, Southwestern Guizhou, China. *Econ. Geol.*, **2022**, 117(5): 1203-1224.
43. Hu Y. Sedimentary basin analysis and study on antimony and gold mineralization in southwest Guizhou Depression. Doctoral degree, *Kunming University of Science and Technology*, Kunming, China, 2011. (In Chinese with English Abstract)
44. Gao W., Hu R., Mei L., Bi X., Fu S., Huang M., Yan J., Li J. Monitoring the evolution of sulfur isotope and metal concentrations across gold-bearing pyrite of Carlin-type gold deposits in the Youjiang Basin, SW China. *Ore Geol. Rev.*, **2022**, 147: 104990.
45. Hu Y., Liu W., Wang J., Zhang G., Zhou Z., Han R. Basin-scale structure control of Carlin-style gold deposits in central Southwestern Guizhou, China: Insights from seismic reflection profiles and gravity data. *Ore Geol. Rev.*, **2017**, 91: 444-462.
46. Tang Y., Zhen L., Li Y., Gao X, Zong W, Sun Q., He D. The aromatic fraction of source rocks from the Jurassic Haifanggou Formation in Niuyingzi Depression of Lingyuan-Ningcheng Basin. *Nat. Gas Geosci.*, **2019**, 30(3): 433-446. (In Chinese with English Abstract)
47. Jiang D., Ji C. Distribution characteristic of aromatic hydrocarbon and the significance of Shenglihe oil shale in Qiangtang Basin. *Contrib. Geol. Miner. Resour. Res.*, **2020**, 35(2): 197-203. (In Chinese with English Abstract)
48. Radke M., Welte D.H., Willsch H. Geochemical study on a well in the Western Canada Basin: relation of the aromatic distribution pattern to maturity of organic matter. *Geochim. Cosmochim. Acta*, **1982**, 46(1): 1-10.
49. Radke M., Rullkötter J., Vriend S. Distribution of naphthalenes in crude oils from the Java Sea: Source and maturation effects. *Geochim. Cosmochim. Acta*, **1994**, 58(17): 3675-3689.
50. Chen Z., Li S., Wang Z. A study on maturity indicators some of some aromatics in low-midmature thermal evolution zones. *Acta Sedimentol. Sin.*, **1997**, (2): 192-197. (In Chinese with English Abstract)
51. Chen Z., Zhang J., Niu L., Gao Y., Zhao C., Wang X. Applicability of aromatic parameters in maturity evaluation of lacustrine source rocks: a case study of Mesozoic source rocks in Yingen-Ejinaqi Basin. *Acta Pet. Sin.*, **2020**, 41(8): 928-939. (In Chinese with English Abstract)
52. Radke M. Application of aromatic compounds as maturity indicators in source rocks and crude oils. *Mar. Pet. Geol.*, **1988**, 5(3): 224-236.
53. Wang C., Zhang H., Li S., Wen L. Maturity parameters selection and applicable range analysis of organic matter based on molecular markers. *Geol. Sci. Technol. Inf.*, **2018**, 37(4): 202-211. (In Chinese with English Abstract)
54. Kvalheim O.M., Christy A.A., Telnæs N., Bjørseth A. Maturity determination of organic matter in coals using the methylphenanthrene distribution. *Geochim. Cosmochim. Acta*, **1987**, 51(7): 1883-1888.
55. Bao J., Wang T., Zhou Y., Yu F., Wang J., Zhou Q., Chen F. The relationship between methyl phenanthrene ratios and the evolution of organic matter. *J. Jiangnan Pet. Inst.*, **1992**: 8-13, 19. (In Chinese with English Abstract)
56. Milner C., Rogers M., Evans C. Petroleum transformations in reservoirs. *J. Geochem. Explor.*, **1977**, 7: 101-153.
57. Chakhmakhchev A., Suzuki M., Takayama K. Distribution of alkylated dibenzothiophenes in petroleum as a tool for maturity assessments. *Org. Geochem.*, **1997**, 26(7): 483-489.
58. Luo J., Cheng K., Fu L., Hu Y., Jiang N. Alkylated dibenzothiophene index— a new method to assess thermal maturity of source rocks. *Acta Pet. Sin.*, **2001**, (3): 27-31, 7. (In Chinese with English Abstract)
59. Dzou L., Noble R., Senftle J. Maturation effects on absolute biomarker concentration in a suite of coals and associated vitrinite concentrates. *Org. Geochem.*, **1995**, 23(7): 681-697.
60. Liu Y., Gang W., Chen G., Sun J., Jiang C. Geochemical characteristics of aromatic hydrocarbons of Chang7 source rocks from the Yanchi-Dingbian area, Ordos Basin. *Acta Sedimentol. Sin.*, **2018**, 36(4): 818-828. (In Chinese with English Abstract)
61. Zhu Y. Thermal evolution and maturity parameters of pentacyclic aromatic hydrocarbons in source rocks. *Geol.-Geochem.*, **1998**, (1): 75-80. (In Chinese with English Abstract)
62. Tuo J. Geochemistry of the tertiary aromatic hydrocarbons in the Qaidam basin — relationship between dicyclic and polycyclic aromatic hydrocarbons. *Exp. Pet. Geol.*, 1996, (4): 406-412. (In Chinese with English Abstract)
63. Alexander R., Larcher A.V., Kagi R.I., Price P.L. The use of plant derived biomarkers for correlation of oils with source rocks in the Cooper/Eromanga basin system, Australia. *Appea J.*, **1988**, 28: 310-324.
64. Zhu Y., Zhang H., Fu J., Sheng G. Distribution and composition of aromatic hydrocarbon in various oils from Tarim basin. *Acta Pet. Sin.*, **1998**, (3): 45-49, 6. (In Chinese with English Abstract)
65. Jiang N, Huang D, Song F., Ren D. Distribution characteristics of aromatics in formations under different sedimentary environments. *Acta Pet. Sin.*, **1994**, (3): 42-50. (In Chinese with English Abstract)
66. Wen Z., Ruiyong W., Radke M., Qingyu W., Guoying S., Zhili L. Retene in pyrolysates of algal and bacterial organic matter. *Org. Geochem.*, **2000**, 31(7): 757-762.
67. Riolo J., Hussler G., Albrecht P., Connan J. Distribution of aromatic steroids in geological samples: their evaluation as geochemical parameters. *Org. Geochem.*, **1986**, 10(4): 981-990.
68. Gschwend P.M., Chen P.H., Hites R.A. On the formation of perylene in recent sediments: kinetic models. *Geochim. Cosmochim. Acta*, **1983**, 47(12): 2115-2119.
69. Zhu Y., Fu J., Sheng G. Geochemical significance of organic sulfur compounds in the Tarim oils. *Exp. Pet. Geol.*, **1998**, (3): 51-55. (In Chinese with English Abstract)
70. Hughes W.B., Holba A.G., Dzou L.I. The ratios of dibenzothiophene to phenanthrene and pristane to phytane as indicators of depositional environment and lithology of petroleum source rocks. *Geochim. Cosmochim. Acta*, **1995**, 59(17): 3581-3598.
71. Pu F., Philip R., Zhenxi L., Guangguo Y. Geochemical characteristics of aromatic hydrocarbons of crude oils and source rocks from different sedimentary environments. *Org. Geochem.*, **1990**, 16(1): 427-435.

72. Zhang M., Philp P. Geochemical characterization of aromatic hydrocarbons in crude oils from the Tarim, Qaidam and Turpan Basins, NW China. *Pet. Sci.*, **2010**, 7(4): 448-457.
73. Li M., Wang T., Zhong N., Zhang W., Sadik A., Li H. Ternary diagram of fluorenes, dibenzothiophenes and dibenzofurans: indicating depositional environment of crude oil source rocks. *Energy Explor. Exploit.*, **2013**, 31(4): 569-588.
74. Jiang L., George S.C. Geochemical comparison of three oil families from the Gippsland Basin, SE Australia. *Mar. Pet. Geol.*, **2020**, 121.
75. Li S., He S. Geochemical characteristics of dibenzothiophene, dibenzofuran and fluorene and their homologues and their environmental indication. *Geochim.*, **2008**, (1): 45-50. (In Chinese with English Abstract)
76. Tang X, Qin W., Qin Q., Gao W., Luo S. Upper Paleozoic group shale gas resources analysis in southwestern Guizhou province. *Coal Geol. China*, **2014**, 26(6): 1-4. (In Chinese with English Abstract)
77. Zhao M, Zhao L., Zhang S., Liu P. Geochemical characteristics of main source rocks in the Nanpanjiang basin. *Exp. Pet. Geol.*, **2006**: 162-167. (In Chinese with English Abstract)
78. Mei M, Ma Y., Dia S., Lv T., Zhang G., Wang G., Tan D. Late Paleozoic filling succession of the Nanpanjiang basin and the division of association of oil generating strata, reservoir and capping bed. *Geosci.*, **2001**, (1): 76-84. (In Chinese with English Abstract)
79. Zhao M., Zhang S., Zhao L., Liu P. Geochemistry and genesis of bitumen in paleo-oil reservoir in the Nanpanjiang Basin, China. *Acta Geol. Sin.*, **2006**: 893-901, 926. (In Chinese with English Abstract)
80. Zhao M., Zhang S., Zhao L., Jiang D. Geochemical features and genesis of the natural gas and bitumen in paleo-oil reservoirs of Nanpanjiang Basin, China. *Sci. China, Ser. D: Earth Sci.*, **2007**, (5): 689-701.
81. Zhang S., Zhao M., Zhang S., Zhao L., Liu P. The genesis and geochemical characteristics of natural gas in well Yang-1 in Nanpanjiang basin. *Nat. Gas Geosci.*, **2005**, (6): 797-803. (In Chinese with English Abstract)
82. Orr W.L. Changes in Sulfur Content and Isotopic Ratios of Sulfur during Petroleum Maturation—Study of Big Horn Basin Paleozoic Oils1. *AAPG Bull.*, **1974**, 58(11): 2295-2318.
83. Fei A., Zhu G., Zhang S., Hu J., Chen S., Zhang B., Su J. Global distribution hydrogen sulphide-bearing natural gas and the major factors controlling its formation. *Earth Sci. Front.*, **2010**, 17(1): 350-360. (In Chinese with English Abstract)
84. Zhu G., Fei A., Zhao J., Liu C. Sulfur isotopic fractionation and mechanism for thermochemical sulfate reduction genetic H₂S. *Acta Petrol. Sin.*, **2014**, 30(12): 3772-3786. (In Chinese with English Abstract)
85. Belenitskaya G.A. Distribution pattern of hydrogen sulphide-bearing gas in the former Soviet Union. *Pet. Geosci.*, **2000**, 6(2): 175-187.
86. Manzano B., Fowler M., Machel H. The influence of thermochemical sulphate reduction on hydrocarbon composition in Nisku reservoirs, Brazeau river area, Alberta, Canada. *Org. Geochem.*, **1997**, 27(7): 507-521.
87. Desrocher S., Hutcheon I., Kirste D., Henderson C.M. Constraints on the generation of H₂S and CO₂ in the subsurface Triassic, Alberta Basin, Canada. *Chem. Geol.*, **2004**, 204(3): 237-254.
88. Heydari E. The role of burial diagenesis in hydrocarbon destruction and H₂S accumulation, Upper Jurassic Smackover Formation, Black Creek Field, Mississippi1. *AAPG Bull.*, **1997**, 81(1): 26-45.
89. Aali J., Rahimpour-Bonab H., Kamali M.R. Geochemistry and origin of the world's largest gas field from Persian Gulf, Iran. *J. Pet. Sci. Eng.*, **2006**, 50(3): 161-175.
90. Carrigan W., Jones P., Tobey M., Halpern H., Wender L., Philip R., Allen J. Geochemical variations among eastern Saudi Arabian Paleozoic condensates related to different source kitchen areas. *Org. Geochem.*, **1998**, 29(1): 785-798.
91. Worden R., Smalley P. H₂S-producing reactions in deep carbonate gas reservoirs: Khuff Formation, Abu Dhabi. *Chem. Geol.*, **1996**, 133(1): 157-171.
92. Baric G., Mesic I., Jungwirth M. Petroleum geochemistry of the deep part of the Drava Depression, Croatia. *Org. Geochem.*, **1998**, 29(1): 571-582.
93. Guangyou Z., Shuichang Z., Liang Y. The origin and distribution of hydrogen sulfide in the petroliferous basins, China. *Acta Geol. Sin.*, **2009**, 83: 1188-1201.
94. Zhu G., Zhang B., Yang H., Su J., Han J. Origin of deep strata gas of Tazhong in Tarim Basin, China. *Org. Geochem.*, **2014**, 74: 85-97.
95. Wenhui L., Tenger, Bo G., Zhongning Z., Jianyong Z., Dianwei Z., Ming F., Xiaodong F., Lunju Z., Quanyou L. H₂S formation and enrichment mechanisms in medium to large scale natural gas fields (reservoirs) in the Sichuan Basin. *Pet. Explor. Dev.*, **2010**, 37(5): 513-522.
96. Elias Bahnan A., Pironon J., Carpentier C., Barré G., Gaucher E.C. The diagenetic history of the giant Lacq gas field, witness to the Apto-albian rifting and the Pyrenean orogeny, revealed by fluid and basin modeling. *Mar. Pet. Geol.*, **2021**, 133: 105250.
97. Luo K., Zhou J., Ju Y. A shift from BSR to TSR caused the formation of the Chipu Pb-Zn deposit, South China. *Ore Geol. Rev.*, **2022**: 104845.
98. Vincent V.I., Li H., Girei M.B., Förster M.W., Ahmed H.A., Ntekim E.E. In situ trace elements and sulfur isotope analysis of sulfides from the Akiri Cu ± (Ag) deposit, Benue Trough, North-central Nigeria: Implications for ore genesis. *Geochemistry*, **2021**, 81(4): 125801.
99. Machel H.G., Krouse H.R., Sassen R. Products and distinguishing criteria of bacterial and thermochemical sulfate reduction. *Appl. Geochem.*, **1995**, 10(4): 373-389.
100. Zhang T., Amrani A., Ellis G.S., Ma Q., Tang Y. Experimental investigation on thermochemical sulfate reduction by H₂S initiation. *Geochim. Cosmochim. Acta*, **2008**, 72(14): 3518-3530.

101. Cai C., Worden R.H., Bottrell S.H., Wang L., Yang C. Thermochemical sulphate reduction and the generation of hydrogen sulphide and thiols (mercaptans) in Triassic carbonate reservoirs from the Sichuan Basin, China. *Chem. Geol.*, **2003**, 202(1): 39-57.
102. Wei Z., Moldowan J.M., Fago F., Dahl J.E., Cai C., Peters K.E. Origins of thiadiamondoids and diamondoidthiols in petroleum. *Energy Fuels*, **2007**, 21(6): 3431-3436.
103. Cai C., Li K., Anlai M., Zhang C., Xu Z., Worden R.H., Wu G., Zhang B., Chen L. Distinguishing Cambrian from Upper Ordovician source rocks: Evidence from sulfur isotopes and biomarkers in the Tarim Basin. *Org. Geochem.*, **2009**, 40(7): 755-768.
104. Wei Z., Walters C.C., Michael Moldowan J., Mankiewicz P.J., Pottorf R.J., Xiao Y., Maze W., Nguyen P.T., Madincea M.E., Phan N.T., Peters K.E. Thiadiamondoids as proxies for the extent of thermochemical sulfate reduction. *Org. Geochem.*, **2012**, 44: 53-70.
105. Zhang S., Huang H., Su J., Liu M., Wang X., Hu J. Geochemistry of Paleozoic marine petroleum from the Tarim Basin, NW China: Part 5. Effect of maturation, TSR and mixing on the occurrence and distribution of alkyldibenzothiophenes. *Org. Geochem.*, **2015**, 86: 5-18.
106. Zhu G., Zhang Y., Zhang Z., Li T., He N., Grice K., Neng Y., Greenwood P. High abundance of alkylated diamondoids, thiadiamondoids and thioaromatics in recently discovered sulfur-rich LS2 condensate in the Tarim Basin. *Org. Geochem.*, **2018**, 123: 136-143.
107. Cai C., Zhao L. Thermochemical sulfate reduction and its effects on petroleum composition and reservoir quality: advances and problems. *Bull. Mineral., Petrol. Geochem.*, **2016**, 35(5): 851-859, 806. (In Chinese with English Abstract)
108. Wang G., Li N., Gao B., Li X., Shi S., Wang T. Thermochemical sulfate reduction in fossil Ordovician deposits of the Majiang area: Evidence from a molecular-marker investigation. *Chin. Sci. Bull.*, **2013**, 58(33): 3450-3457. (In Chinese with English Abstract)
109. Yuan Y., Wang T., Cai C, Xu C, Qin Q. Relationships between sulfur-containing compound types in crude oil and causes of thermochemical sulphate reduction in Tazhong area. *J. Southwest Pet. Univ., Sci. Technol. Ed.*, **2020**, 42(2): 48-60. (In Chinese with English Abstract)
110. Cui H., Wang F., Wang Q., Xu P., Sun L. Geochemical characteristics of aromatics from source rocks in Miaoxibei Sag, Bohai Sea area, China. *J. Chengdu Univ. Technol., Sci. Technol. Ed.*, **2021**, 48(6): 653-660. (In Chinese with English Abstract)
111. Wang J., Bai J., Li X., Liu P., Wang B. Geochemical characteristics of aromatic hydrocarbon of crude oil from Chi'an Oilfield in Gaoyou Sag. *Complex Hydrocarbon Reservoirs*, **2015**, 8(4): 23-26, 30. (In Chinese with English Abstract)
112. Xu T., Hou D., Cao B., Chen X., Diao H. Characteristics of aromatic geochemistry in light oils from Xihu Sag in East China Sea Basin. *Acta Sedimentol. Sin.*, **2017**, 35(1): 182-192. (In Chinese with English Abstract)